JWW

Validation of UARS MLS 183 GHz H_2O Measurements

W.A. Lahoz[4], M.R. Suttie[1], J. Froidevaux[2], R.S. Harwood[1], C.L. Lau[3]

T. A. Lungu[2], G.E. Peckham[3], H.C. Pumphrey[1], W.G. Read[2]

Z. Shippony[2], R. A. Suttie[3], J.W. Waters[2], G. E. Nedoluha[5]

S.J. Oltmans[6], J.M. Russell III[7], W. A. Traub[8]

[1] Edinburgh University, Edinburgh, Scotland, UK.

[2] Jet Propulsion Laboratory, Pasadena, CA, USA.

[3] Heriot-Watt University, Edinburgh, Scotland, UK.

[4] CGAM, Reading University, Reading, England, UK.

[5] Naval Research Laboratory, Washington, DC, USA.

[6] NOAA CMDL, Boulder, CO, USA.

[7] NASA Langley Research Centre, Hampton, VA, USA

[8] Harvard-Smithsonian Centre for Astrophysics, Cambridge, MA, USA.

2nd March 1995

Abstract. The Upper Atmosphere Research Satellite (UARS) Microwave Limb Sounder (MLS) makes measurements of thermal emission at 183.3 GHz which are used to infer the concentration of water vapour over a pressure range of 46 hPa to 0.2 hPa ($\sim$ 20 km to $\sim$ 60 km). We provide a validation of MLS H_2O by analysing the integrity of the measurements, by providing an error characterization and by comparison with data from other instruments. It is estimated that Version 3 MLS H_2O retrievals are accurate to within 20-25 % in the lower stratosphere and to within 8-13 % in the upper stratosphere and lower mesosphere.

The precision of a single profile is estimated to be $\sim$ 0.15 ppmv in the mid-stratosphere and 0.2 ppmv in the lower and upper stratosphere. In the lower mesosphere the estimate of single profile precision is 0.25–0.45 ppmv. During polar winter conditions H_2O retrievals at 46 hPa can have a substantial contribution from climatology. The vertical resolution of MLS H_2O retrievals is $\sim$ 5 km.

1. Introduction

The Upper Atmosphere Research Satellite (UARS) was launched on 12 September 1991 carrying a payload to measure the chemistry, dynamics and energy balance of the middle atmosphere [*Reber, 1990*]. This paper concerns the data validation of middle atmosphere distributions of H_2O as measured by the Microwave Limb Sounder (MLS) [*Barath et al., 1993; Waters, 1993*].

The MLS instrument is a joint USA-UK experiment employing a three radiometer design, with a 183 GHz radiometer built in the UK that measures H_2O using the emission from the 183.3 GHz H_2O line and O_3 using the emission of the 184.4 GHz O_3 line. For details of the spectroscopy of these two lines see Waters [*1976, 1993*]. This paper discusses the MLS H_2O measurements and their validation, concentrating on the Version 3 MLS data files, the first version to be made publicly available. Companion papers describe the calibration of the MLS instrument [*Jarnot et al., 1994*], the 'forward model' [*Read et al., paper in preparation*], and validation of MLS ClO [*Waters et al., 1994*], O_3 [*Froidevaux et al., 1994*] and temperature and tangent-point pressure [*Fishbein et al., 1994*]. *Froidevaux et al. [1994]* give a description of the general algorithms used for retrieving parameters from the calibrated MLS radiances.

In the following sections we provide validation of MLS H_2O data by discussing data

cessing and the integrity of the radiances used in the retrieval process, by performing an error analysis and by making comparisons between MLS H_2O and other measurements. On the basis of these studies we provide estimates of the accuracy and precision of MLS H_2O data. We also discuss outstanding issues and further work associated with this data set.

2. MLS Version 3 Data Processing

The output of the 183 GHz radiometer is down-converted through an Intermediate Frequency (IF) stage into a 15 channel, 500" MHz wide filter-bank, centred on the 183.3 GHz line. The measured radiances include the contributions of a primary sideband and an image sideband [*Jarnot et al., 1994*]. From the intensity and spectral characteristics of this emission and its variation as the MLS field of view (FOV) is scanned vertically across the atmospheric limb, profiles of H_2O are inferred. The width of the MLS FOV half-power points is 3.7 km in the vertical and 7.2 km in the horizontal. The horizontal resolution along the line of sight (perpendicular to the UARS velocity vector) is $\sim$ 400 km, set by the physics of radiative transfer.

The measurement latitudinal coverage is from 34° on one side of the equator to 80° on the other. UARS yaws around at $\sim$ 36 day intervals (a 'UARS month'), when MLS high latitude coverage switches from one hemisphere to the other. Within each UARS month, the UARS orbit precesses slowly with respect to local solar time, so that the measurements sweep through all local solar times during a UARS month, coming $\sim$ 20 minutes earlier each day at a fixed latitude.

The UARS project has defined four levels of data (Level 0 $\rightarrow$ Level 3) which represent the data flow from raw telemetry data, Level 0, to fields of geophysical parameters on

standard grids, Levels 3AT, 3AL and 3B. UARS Level 1 data consist of calibrated radiances for each channel, their measurement precisions, and related instrument data. The MLS radiance values are expressed as brightness temperatures in units of degrees Kelvin and have a random uncertainty associated with them. UARS Level 2 data consist of geophysical parameters, and numerous diagnostics. The UARS Level 2 data are on a grid chosen by each instrument team. MLS Level 2 data consist of vertical profiles (the vertical coordinate being $-\log_{10}(p)$, p being pressure in hPa) of geophysical parameters which have a spatial and temporal location associated with them. The retrieval algorithm used to derive Level 2 data is based on a combination of *a priori* and measurement information [*Rodgers, 1976; Froidevaux et al., 1994*] and makes use of the forward model, developed by *Read et al.* [*paper in preparation*], to calculate the influence functions (also known as weighting functions). It is clear that the integrity of the Level 2 and Level 3 data is very dependent on the integrity of the Level 1 radiances and considerable effort has been expended in assessing the robustness of these radiances [*inter alia Jarnot et al., 1994*]. More details will be provided in section §3.1.0.10W.

UARS Level 3AT data are geophysical parameters gridded each 65.536 s time interval onto pressure surfaces p_n, where $p_n = 1000 \times 10^{-n/6}$ hPa ($n = 0, \ldots, 42$) (which would correspond to a constant height spacing of 2.7 km in an isothermal atmosphere with a constant pressure scale-height of 7 km). Each day contains 1318 or 1319 profiles. The MLS Level 3AT retrieved water vapour volume mixing ratio profile is represented as a piecewise-linear function with breakpoints at alternate, even numbered, UARS pressure surfaces, e.g. at 10, 4.6, 2.2 and 1 hPa. (The MLS Level 2 retrieved profiles are similarly represented.) The water vapour mixing ratios on the even-numbered surfaces are the retrieved breakpoint

ues, while those on the odd-numbered surfaces, e.g. 6.8, 3.2 and 1.5 hPa, are averages of the mixing ratios on adjacent even-numbered surfaces. This means that the vertical resolution of Level 3AT H_2O profiles imposed by this representation corresponds to a height resolution of $\sim$5.4 km, Level 3AL data are like 3AT data except gridded every 4° in latitude and temporal information is lost. There are generally only about 2/3 the number of Level 3AT profiles in a Level 3AL file, namely close to 840 profiles. The Level 3B data comprise globally mapped representations of 3AL data.

Retrievals of MLS data are constrained with *a priori* information, with the result that, where there is poor information content in the MLS measurements, the retrieved values and their associated uncertainties relax to the *a priori* values. Consequently, it is important for the retrieval algorithm to have reasonable *a priori* inputs (values and error information) so that they do not over-constrain or under-constrain the solution.

In the case of MLS, the *a priori* inputs (or 'climatology') are based on a month-dependent climatology developed by the UARS science team *[inter alia MAP Handbook 31, 1989]*. The UARS H_2O climatology *[Remsberg et al., 1990]* consists mainly of monthly zonal means from the Limb Infrared Monitor of the Stratosphere (LIMS) *[Russell et al., 1984]* for seven months (November May), 100 hPa to 1.5 hPa and 56°S to 84°N. From 1.5 hPa to 0.5 hPa, radiance averaged profiles from LIMS data are used. Besides the LIMS data, ground-based microwave data [see, for example, *Bevilacqua et al., 1985, 1987; Tsou et al., 1988*] are used in the mesosphere for pressures of 0.5 hPa to 0.01 hPa. The 1990 UARS climatology was extended to the whole of the year by assuming hemispheric symmetry in the seasons. Extensions where UARS climatology is unavailable make use of default values which were constructed from the Caltech/JPL photochemical model for a mid-latitude equinox day. A diagonal *a*

priori error covariance matrix is used. In the stratosphere the assumed *a priori* uncertainty is set to 2 ppmv. By comparison, the standard deviation about the zonal mean of typical LIMS H_2O profiles for May and October tends to be less than 1 ppmv throughout most of the stratosphere [*Remsberg et al., 1990*]. This strongly suggests that an *a priori* error of 2 ppmv for MLS H_2O retrievals ill the stratosphere is large and is unlikely to overconstrain the solution to the input climatology. Tests with significantly larger *a priori* errors gave results which were negligibly different from the standard retrievals within the useful vertical range of the data.

The uncertainty, σ, associated with each retrieved H_2O profile is computed by the retrieval algorithm and is stored along with the retrieved value in the Level 2 and Level 3 files as a quality indicater. This uncertainty, which includes contributions from random noise and from certain systematic errors, is obtained by propagating the precisions of the radiance measurements (a Level 1 product), the estimates of uncertainties in the constrained parameters and the estimates of inaccuracies in the forward model through the retrieval software. A more detailed discussion]] of the errors associated with Version 3 MLS H_2O retrievals is presented in sections § 3 and 4.

At the conclusion of the retrieval, the ratio of the estimated uncertainty to its *a priori* counterpart is formal. This ratio is sometimes termed the 'error ratio'. When this ratio exceeds 0.5 (i.e. the retrieved mixing ratio has a contribution from the climatology which exceeds 25 %) the quality is set negative to flag the dependence of the retrieval on the climatology. Typically, for every profile, this tends to occur at or above the 0.046 hPa retrim'al level and below 46 hPa. However, at high latitudes in winter, the ratio can exceed 0.5 at 46 hPa and at 22 hPa (see section § 6).

An important feature of the UARS MLS experiment is that it measures O_3 at two different frequencies (1 84.4 GHz and 206.1 GHz) using two different radiometers (183 GHz and 205 GHz). In regions of the atmosphere where both measurements are sensitive to changes in constituent amount, the availability of two independent O_3 measurements means that intra-MLS comparisons can be carried out and, for example, the consistency of the calibration of the 183 GHz and 205 GHz radiometers can be checked. The Version 3 algorithms contain an adjustment to the pointing angle of the 183 GHz radiometer field of view (FOV), based on a comparison between the two ozone retrievals and in-flight calibration involving scans across the disk of the moon [*Froidevaux et al., 1994*]. This has had an impact on the MLS H_2O distribution, namely a reduction of $\sim$ 5% in retrieved stratospheric values by comparison with Version 2 retrievals.

The MLS radiances can contain an offset, or baseline, which is caused by a variety of effects such as insufficiently accurate modelling of the sidelobes of the antenna FOV. It does not depend on frequency, but can change from one tangent height to the next. The baseline is handled by retrieving it along with the water vapour. The *a priori* value of the baseline is taken to be the retrieved value for the tangent height above the one being retrieved. The *a priori* uncertainty for the baseline is 3 K. Above 40 km, where there should be little or no signal in the wing channels, the baseline can be retrieved very accurately. It usually has a value of about 2 K at 80 km dropping to 1.5 K at 40 km. In the lower stratosphere, it becomes difficult to distinguish between baseline effects and radiation which is due to water vapour. The retrieved baseline often increases sharply to between 4 K and 8 K in this region. This may be a source of systematic error in the water vapour retrieval in the lower stratosphere and is a subject of current investigation.

The Version 3 retrieval algorithm assumes linearity. Accordingly, it is less accurate in regions where the atmosphere is optically thick and the radiative transfer equations are correspondingly non-linear. The 183.3 GHz H_2O emission line measured by MLS is relatively strong and, consequently, tends to have high opacities throughout the stratosphere: the line centre becomes optically thick for levels in and below the upper stratosphere; the wings of this line become optically thick for levels in and below the lower stratosphere. Furthermore, no tropospheric retrievals of H_2O are possible with the 183 GHz radiometer due to limited bandwidth. To prevent the retrieval algorithm from operating in regimes that are non-linear, an 'opacity criterion' [*Froidevaux et al., 1994*] has been devised to discard measurement information when the estimated optical depth exceeds a value of 1.0.

Investigations on the data quality of Version 3 MLS H_2O provide strong evidence that retrievals at the 46 hPa level at high latitudes in winter can have a substantial contribution from the *a priori* input. Detailed studies indicate that this is due to a combination of the atmosphere being optically thick and the very low temperatures prevailing in these regions (especially in winter), which results in estimated opacities for these cases exceeding the 'opacity criterion' and a consequent loss of information content. In these circumstances most of the information is contributed from fields of view with tangent pressures less than 46 hPa.

3. Signals and Closure

In this section we discuss the integrity of the radiances measured by band 5 of the MLS 183 GHz radiometer. We present a test of consistency and investigate the extent of closure of these radiances. We also discuss closure issues for the retrieved H_2O mixing ratios by

means of simulated retrievals.

3.1 Radiances

An important aspect of validating the MLS H_2O retrievals is the examination of the radiances measured by the instrument. Figure 1 shows calculated limb emission in the spectral region 182- 187 GHz which includes both spectral sidebands of band 5 and band 6 (MLS band 6 radiances are used for retrieving O_3, see *Froidevaux et al., 1994*). The position of the local oscillator (LO) at 184.78 GHz is indicated on the plot. Spectra are shown for tangent pressures in both the upper and lower stratosphere. Spectral lines of all molecules which are thought to be important are included in the calculation employing spectral data from the JPL catalogue [*Pickett et al., 1992*]. The primary (signal) sideband is dominated by the 183.3 GHz H_2O line whereas the image sideband contains no strong lines, giving a 'clean' measurement of 183 GHz H_2O limb emission. There are 15 spectral channels spanning the 510 MHz bandwidth of band 5. For each channel the *sideband ratio*, describing the relative response of the primary and image sidebands, has been measured. Details of the bandwidth and frequencies of the channels, of the vertical scan patterns and of the procedures for converting the Level 0 data to calibrated radiances and error estimates (Level 1 data) are given in *Jarnot et al.*, [*1994*]. On 31 st October 1991, the vertical resolution of the scan pattern was increased in the lower stratosphere to improve measurements in this region.

Typical examples of measured radiances in band 5 are shown in Figures 2 and 3. Vertical profiles of the radiances in channels 1 to 8 are plotted in Figure 2. Channel 8 measures the limb emission at the line centre and saturates in the primary sideband at tangent heights of $\sim$ 50 km. Between $\sim$ 50 km and $\sim$ 20 km, where the primary sideband of channel 8 is

saturated and there is no significant signal in the image sideband, variations in that radiance reflect variations in the temperature of the atmosphere. For channel 1, on the wing of the 183.3 GHz line, the signal in the primary sideband is not significant until the FOV is scanned down to tangent heights of ~ 30 km. The signal in the image sideband begins to make a significant contribution in all channels at ~ 20 km. The three panels in Figure 3 display typical measured spectra in the mesosphere, 11])])('1" stratosphere and lower stratosphere. The width of each channel is depicted by a horizontal bar and the 1σ measurement uncertainty is represented by a vertical bar. The effect of pressure broadening is clearly seen as the tangent pressure increases.

3.2 Internal Consistency

In an isothermal atmosphere, when a spectral channel is saturated, the radiance in that channel should represent the black-body emission for the temperature of the atmosphere and is insensitive to the amount of atmospheric constituent. One test of consistency of the measured radiances is to compare them with the retrieved temperatures for a profile which is nearly isothermal. Figure 4 shows the radiances for such a profile, with the temperature also plotted and scaled by the sideband ratio. The radiances behave qualitatively as expected; all channels appearing to saturate within 10 K of a brightness temperature of approximately 1251<. The center channels saturate at a slightly higher temperature because the profile is not quite isothermal; the temperature increases slightly with height. The saturation is less clear in the wing channels because the image sideband starts to receive radiation at tangent heights where the principal sideband is not saturated.

It is clear, however, that the measured radiances tend to saturate at a brightness tem-

perature between 5 and 10 K higher than the temperature profile would lead one to expect. Approximately 1 K of this discrepancy is due to a systematic bias in the MLS temperature retrieval(see *Fishbein et al., 1994*); another 2 K is the baseline. The rest is possibly due to inexact knowledge of the sideband ratios. The effect this would have on the Version 3 retrieval is small, because radiances close to saturation are not used, while those far from saturation are not too sensitive to sideband ratio. 110WCVCV, it is necessary that we resolve this discrepancy before a full nonlinear retrieval can be carried out.

3.3 Closure in Radiances

Another test of a retrieval scheme is the extent to which radiances calculated from the retrieved product agree with the measured radiances within the expected noise. Discrepancies larger than instrument noise indicate a lack of adequate fit to the measured radiances and indicate some type of systematic error. The source of this error could either be in the retrieved product or in the forward model which calculated the radiances. We define the *radiance residual* as the measured radiance minus the calculated radiance, and the nature of the variation of these residuals with respect to height, spectral channel and location is discussed.

The plots in Figure 5 show typical variations of radiance residual with height, for each of the 15 channels of band 5, for an equatorial location on 10th January 1992. The horizontal bars represent the 1σ measurement noise. The plots in Figure 5 relate to a single profile, but they are representative of the generally observed variation of radiance residual with height. Figures 6 and 7 show plots of average residuals within latitude bands 10°N- 10°S and 60°N-80°N, respectively, for 10th January 1992. Each of these figures displays the variation of

the average residuals within eight selected pressure bins ranging from 100 hPa to 0.01 hPa. Vertical bars represent the standard error on the mean measured radiance for a particular channel within a particular pressure range and latitude band. In general, this quantity is small and due to the vertical scale of the plots in Figures 6 and 7 these vertical bars are visible in the pressure range 0.032- 0.01 hPa only. The number of limb views which were included in each of the calculations of the average residual ranges from around 200 for the pressure range 0.032- 0.01 hPa to about 800 for the pressure range 100- 31.6 hPa. Within the two latitude bands mentioned above, similar variations of average residual with spectral channel are found, except for channels 7 and 8 in the mesosphere.

The main features of the residuals in Figures 5- 7, are as follows. A large negative residual of $\sim$ - 15 K (10- 15 %) appears in all channels at around 15 km (see Figure 5). At this level in the atmosphere, the Version 3 MLS H_2O retrievals provide essentially no measurement information and *a priori* abundances are climatological. If the *a priori* H_2O amount is an overestimate of the truth at around 15 km, then the recalculated radiances will be greater than the measured radiance which would result in a negative residual. This occurs below the lower limit of the useful vertical range for MLS Version 3 H_2O retrievals (see Section § 4).

Referring to Figures 6 and 7, certain systematic patterns are evident in the spectral signature of the residuals. In the lower stratosphere there appears to be an asymmetry in the residuals for the wing channels. In the pressure range 31.6- 10 hPa channels 13, 14 and 15 exhibit negative residuals whereas the residuals in channels 1, 2 and 3 are positive. Channels 4- 11 have positive residuals of between 2- 4 K (1- 4 %) in the latitude bin 10°N- 10°S and smaller positive residuals of 1- 2 K ($\sim$ 1 %) in the latitude bin 60°N- 80°N. These residual

patterns may be the result of a combination of errors in parameters such as the antenna transmission or the relative response of the primary and image sidebands. In the upper stratosphere and lower mesosphere (panels for pressure ranges 10- 3.16 hPa, 3.16- 1 hPa and 1- 0.32 hPa) there appears to be an oscillatory behaviour of the residuals across the band. This signal may be related to errors in the assumed line shape and is under investigation. In the pressure range 0.32- 0.1 hPa the residual pattern differs between the latitude bins 10°N- 10°S and 60°N- 80°N. For this pressure range, channel 9 exhibits a large positive residual in both latitude bins, however, channels 7 and 8 switch from having positive residuals in the range 10° - 10°S to having negative residuals in the 60°N- 80°N range. Residuals for ascending and descending parts of orbits were looked at separately to check whether this effect was due to a Doppler shift caused by winds which are not modelled. However, there was no significant difference in the patterns of residuals between ascending and descending sides of the orbits.

This section has described the main systematic features which occur in the residuals for MLS Version 3 H_2O retrievals. The possible sources of these features, including errors in antenna transmission, assumed line shape, sideband ratios, and the alignment of the field of view are being investigated.

3.4 Closure of retrievals

We now investigate the extent of closure of the MLS Version 3 H_2O retrievals in order to estimate the magnitude of 'numerical errors' arising from the software used to create the Version 3 data files. This involves performing a retrieval using simulated radiances which are calculated from an assumed H_2O distribution. The retrieved H_2O field is then compared

with the original (true) field. In this work, we have employed a smoothed version of the H_2O distribution as retrieved by MLS for 17th September 1992 as the true distribution. Simulated radiances were produced based on this field and these radiances, with simulated noise added, were then used as input to the retrieval. We do not expect perfect closure as the retrieval is based on assumptions of linearity and does not fully utilise the set of radiance measurements when the atmosphere is deemed to be optically thick. This is particularly important for limb views with tangent heights in the lower stratosphere.

The zonal mean of the smoothed H_2O field employed as the true distribution and the zonal mean of the retrieved H_2O field are displayed in panels (a) and (b) of Figure 8, respectively. The zonal mean difference between these two fields is plotted in panel (c) of Figure 8, and the root-mean-square (rms) difference is shown in panel (d). The vertical range of the plots has been limited from 46 hPa to 0.2 hPa. Below 46 hPa the retrieved values are climatological and above 0.2 hPa there exist known problems with the retrieval (see section § 6).

The rms difference between the true and the retrieved H_2O distributions is approximately 0.2 ppmv (2-5 %) throughout the stratosphere with the retrieval having the tendency to overestimate the true distribution in the lower stratosphere. At latitudes greater than 60° (in either hemisphere), on the 46 hPa retrieval surface the rms difference can be larger than 0.6 ppmv (~15 %). This is caused by a loss of measurement information due to estimates of large optical thickness in these regions, and this results in the retrieved values having a substantial contribution from the *a priori*. Above 1 hPa the zonal mean difference remains at ~ 0.2 ppmv (~ 4 %), but the rms difference increases from ~ 0.3 ppmv (~ 5 %) at 1 hPa to nearly 1 ppmv (~ 12 %) at 0.2 hPa. This is due mainly to an increase in random errors,

such as radiance noise and uncertainty in the retrieved temperature, and to an increase in the step size of the FOV scan.

In general, the closure of the retrievals is satisfactory throughout the stratosphere, and the above mentioned features are subjects of current investigation (see section § 6). The error analysis presented in section § 4 takes account of numerical errors produced by the retrieval process.

4. Estimated Uncertainties

In this section we present the estimated uncertainties for the Version 3 MLS H_2O retrievals from band 5 of the 183 GHz radiometer. The estimated uncertainties are based on everything known apart from comparisons with other data sets (see section § 5). We also include information on the averaging kernels (defined below) and vertical resolution of the retrievals. Firstly, a brief review of the method of error characterization is given. This is followed by a discussion of the averaging kernels and vertical resolution, and then estimates of the random uncertainties (precision) and systematic uncertainties are presented.

4.1 Characterization method

A general method for estimating the different contributions to the total uncertainty in retrieving an atmospheric constituent profile by any inversion technique is given by *Rodgers [1990]* (see also *Marks and Rodgers, 1993*). A brief outline of the method is presented below.

If the vector $\mathbf{x}$ represents the true state of the atmosphere and the vector $\hat{\mathbf{x}}$ is the retrieved state then the total error in a retrieval is given, to first Order in small quantities, by

$$\hat{\mathbf{x}} - \mathbf{x} = [T(\bar{\mathbf{x}}, \hat{\mathbf{b}}, \hat{\mathbf{c}}) - \bar{\mathbf{x}}] + \mathbf{D}_y \mathbf{K}_b \epsilon_b + \mathbf{D}_y \epsilon_y + (\mathbf{A} - \mathbf{I})(\mathbf{x} - \bar{\mathbf{x}}), \quad (1)$$

where

$\bar{\mathbf{x}}$ is the reference state of the atmosphere (for MLS $\bar{\mathbf{x}} = \mathbf{x}_a$, the *a priori* state),

$\hat{\mathbf{b}}$ is an estimate of non-retrieved forward model parameters $\mathbf{b}$,

$\hat{\mathbf{c}}$ is an estimate of the inverse model parameters $\mathbf{c}$, e.g. *a priori* data,

the matrix $\mathbf{K}_b$, known as the model parameter *influence function*, is the sensitivity of the model radiances to the forward model parameter vector $\mathbf{b}$,

ϵ_b is the vector of uncertainties in $\mathbf{b}$,

ϵ_y is the measured radiance error vector.

The *transfer function*, T, relates the retrieved state $\hat{\mathbf{x}}$ to the unknown true state $\mathbf{x}$ by $\hat{\mathbf{x}} = T(\mathbf{x}, \mathbf{b}, \mathbf{c})$.

The *contribution function*, $\mathbf{D}_y$, is the sensitivity of the retrieval to the measurements $\mathbf{y}$.

The *averaging kernel* matrix, $\mathbf{A}$, is defined by

$$\mathbf{A} = \frac{\partial \hat{\mathbf{x}}}{\partial \mathbf{x}} = \mathbf{D}_y \mathbf{K}_x,$$

where $\mathbf{K}_x$ is the influence function (also known as the weighting function) matrix of the atmospheric state, i.e. the sensitivity of the model radiances to a change in the state of the atmosphere.

Each row of the matrix A represents the vector of weights by which the true profile is multiplied to give the element of the retrieved profile corresponding to that row. For

an ideal observing system , A would be the identity matrix 1, but normally the rows of A will represent peaked functions, with the width of the peak being a measure of the vertical resolution of t he retrieval .

An e xpression for the total er ror covariance, $\mathbf{S}_T$, of a retrieval is given, from equation (l), as

$$\mathbf{S}_T = \mathbf{S}_P + \mathbf{S}_M + \mathbf{S}_S,$$

where

$$\begin{aligned}
\mathbf{S}_P &= \mathbf{D}_y \mathbf{K}_b \mathbf{S}_b \mathbf{K}_b^T \mathbf{D}_y^T, \\
\mathbf{S}_M &= \mathbf{D}_y \mathbf{S}_\epsilon \mathbf{D}_y^T, \\
\mathbf{S}_S &= (\mathbf{A} - \mathbf{I}) \mathbf{S}_a (\mathbf{A} - \mathbf{I})^T.
\end{aligned}$$

The matrix $\mathbf{S}_P$ is the contribution to the retrieval error covariance of uncertainties in the model parameters, $\mathbf{S}_b$ is the error covariance matrix for the forward model parameters. The matrix $\mathbf{S}_M$ is the contribution of measurement noise to the retrieval error covariance, $\mathbf{S}_\epsilon$ is the measurement error covariance. The matrix $\mathbf{S}_S$ is known as the 'smoothing' error. This can be regarded as the error that comes from the *a priori* error. The matrix $\mathbf{S}_a$ represents the expected covariance of the departures of the true atmosphere from the *a priori* profile.

The method outlined in the above paragraphs has been applied to the Version 3 H_2O retrieval from band 5 of MLS for a typical mid-latitude case. Some important features of the calculations are mentioned and then a discussion of the results of this formal error characterization is given.

The influence functions ($\mathbf{K}$ matrices) were calculated for a typical mid-latitude atmosphere using the formulation of *Read et al.,* [*paper in preparation*], and were evaluated at

43 tangent pressures between $z = -3$ and $z = +4$ inclusively, with a separation in z of 1/6, where z is $-\log_{10}(p)$, p being pressure in hPa. These influence functions were then linearly interpolated onto a typical MLS scan pattern before the error calculations were performed. The retrieval levels chosen for H_2O were the same as those employed by the MLS Version 3 retrieval, i.e., 20 levels between $z = -3$ and $+3.33$ inclusively, with a separation of 1/3.

Typical *a priori* profile uncertainties used by the MLS retrieval were used to construct a purely diagonal covariance matrix, $\mathbf{S}_a$, which therefore assumes that no inter-level correlations are present. The measurement error covariance matrix, $\mathbf{S}_\epsilon$, was constructed from typical MLS band 5 radiance errors under the assumption that no inter-channel correlations are present. The use of an opacity criterion (see section § 2) has also been built into the calculations. When estimating the extent of systematic errors in H_2O mixing ratio, for some systematic effects an equivalent error in radiance was estimated and a corresponding radiance error covariance matrix was constructed, i.e. essentially providing an estimate of $\mathbf{K}_b\mathbf{S}_b\mathbf{K}_b^T$. This error in radiance was then translated into an uncertainty in retrieved H_2O mixing ratio. For other systematic effects an estimate of the root-mean-square (rms) uncertainty in H_2O mixing ratio was given directly from sensitivity studies.

4.2 Averaging kernels and vertical resolution

We now discuss the MLS H_2O averaging kernels. Figure 9 shows the resulting rows of the averaging kernel matrix for the 190 retrieval at levels $z = 2$ to $+3.33$. The number printed at the peak of the functions represents the retrieval level, in $\log_{10}(p)$ (pressure in hPa), associated with each averaging kernel.

In general, between $z = 1.67$ and $+2$ (46 - 0.01 hPa), the averaging kernels are well-

peaked functions with the peak coinciding with the level of the retrieval. In this region most of the information in the H_2O retrieval comes from the measurements and not from the *a priori* information. Below z = - 1.67 (46 hPa), the averaging kernels are not so well peaked because there is little information in the measurements due to the band 5 channels becoming optically thick in this region. Above z = + 2 (0.01 hPa), the averaging kernels become wider and have smaller peaks due to the decreasing signal-to-noise ratio with altitude and the coarser steps of the FOV scan in this region.

As an estimate of the vertical resolution of the MLS Version 3 H_2O retrievals, the 'width' of each averaging kernel has been calculated using the Backus-Gilbert definition of spread [*Backus and Gilbert, 1970*] and is plotted in Figure 10. This gives the vertical resolution between z = 1.33 and + 0.67 (21.5 0.2 hPa) as ~ 5 km and from z = + 1 to + 2.67 (0.1 - 0.(mill'a) as ~ 6-10 km. The vertical resolution at z = -1.67 (46 hPa) is ~ 6 km.

From the information given by the averaging kernels alone, the useful vertical range for Version 3 H_2O retrievals would be 46- 0.01 hPa. However, other evidence, namely frequently-occurring high values at ~ 0.1 hPa which seem unrealistic, leads us to believe that the current useful vertical range is 46- 0.2 hPa for Version 3 data.

4.3 Estimated Precision

We present three methods used to estimate the precision of the H_2O retrievals.

Method 1

This estimate of the precision is based on the formal analysis discussed above. The precision estimate is given by the root-sum-square of the random contributions to the retrieved

H_2O uncertainty which includes the measurement noise, the random errors in retrieved temperature and tangent pressure and uncertainties in other state vector parameters which affect the H_2O retrieval. Figure 11 shows a plot of the dominant random errors together with the root-sum-square (rss) of the random errors. In the lower stratosphere the random error is dominated by the uncertainty in the retrieved tangent pressure. However, the uncertainties in retrieved tangent pressure that are incorporated into the formal error analysis include some systematic effects [*Fishbein et al., 1994*]. Therefore, this method may lead to an overly pessimistic estimate of precision especially in the lower stratosphere. A comparison of this precision estimate with the precision estimates provided by methods 2 and 3 below is shown in Figure 12.

Method 2

This method involves calculating the variability of retrieved profiles near the orbit turning points (near 80°N or 80°S) in the summer hemisphere. It is at these latitudes that the densest sampling occurs and the summer hemisphere is chosen to minimise any effects from atmospheric variability. The line labelled (2) in Figure 12 shows the rms difference between pairs of profiles near the turning points. These profile pairs are less than 2 hours apart in time and are separated by less than 150 km. The time period used was 19th July 1992 to 8th August 1992 which gave 241 pairs of profiles near to 80°N.

Method 3

This method involves calculating the variability of retrieved profiles in the tropics where the atmospheric variability is usually small. The line labelled (3) in Figure 12 shows this

estimate of precision. It is a result of calculating the standard deviation of retrieved profiles in the latitude range 5°N-5°S for each one of 442 days and averaging the standard deviations over these days.

Comparing the precision estimates shown in Figure 12 arising from the three methods described above, we can see that methods 2 and 3 give very similar results, Method 1 gives a poorer estimated precision in the lower stratosphere and this may be related to the presence of systematic components in the retrieved tangent pressure uncertainty as mentioned above. An estimate of the precision for the useful vertical range of the H_2O retrievals is given in Section § 7. Note that the H_2O uncertainties given in the MLS Version 3 data files are somewhat greater than the estimates produced by the above methods. This is mainly because the MLS Version 3 uncertainties contain a contribution from the *apriori* error. This effect is strongest in the lows stratosphere. The MLS Version 3 errors also contain a systematic component which accounts for known differences between linear and nonlinear retrievals.

4.4 Estimated systematic uncertainties

In addition to random uncertainties, it is necessary to consider systematic uncertainties. Figure 13 shows the dominant systematic uncertainties along with the root-sum-square of all the systematic uncertainties considered. Below, we briefly discuss the various error sources which were considered in this analysis. Firstly we will discuss the sources of the dominant systematic uncertainties (see Figure 13).

tangent pressure: Since the retrieved mixing ratios are based on radiances at the retrieved tangent pressure then errors in tangent pressure can produce errors in mixing

ratio. Sensitivity tests were performed assuming a systematic error in tangent pressure of about 6 % [see *Fishbein et al., 1994*]. The main source of this systematic error is from possible errors in the O_2 spectroscopic data base. We can see from Figure 13 that these errors tend to dominate the systematic error between 2 hPa and 0.2 hPa.

temperature: Errors in temperature can lead to errors in mixing ratio. Sensitivity tests were performed taking biases in temperature to be 2 K for latitudes equatorward of 60 degrees and 5 K for latitudes polewar d of 60 degrees. These biases are consistent with observed average differences between MLS and NMC temperatures [see *Fishbein et al., 1994*]. Tangent pressure was retrieved while the temperature biases were imposed. The resulting changes in H_2O mixing ratio were then analysed. Mid-latitudes the systematic uncertainty in mixing ratio is generally about 1- 2 % for a 2 K systematic error in temperature.

retrieval numerics: this refers to the differences between the mixing ratio profiles used to create simulated noise-free radiances, and the subsequent retrieved profiles based on these radiances using the inversion algorithm. At 0.1 hPa (outside the useful vertical range) this uncertainty is ~ 27 % which may account for the unrealistically high mixing ratios which can sometimes occur at this pressure level.

radiance scaling: three sources of scaling errors in calibrated radiances are radiometric calibration, sideband ratio errors and spectroscopic errors in linestrength. The first two error sources are discussed by *Jarnot et al.* [*1994*]. Based on this reference, we use a systematic uncertainty of 0.6 % for the radiometric calibration of the 183 GHz radiometer which corresponds to about one-third of the worst-case error expected. This uncertainty is due mainly to uncertainties in the pre-launch characterisation of losses through the MLS antenna and switching mirror. A covariance matrix of radiance errors from this sourer was

constructed which assumes the errors are fully correlated across the band and with height. Errors in the sideband ratios can lead to possible errors in single sideband radiance of $\sim$ 2 % for the 183 GHz H_2O band [see *Jarnot et al., 1994*] . These errors should be correlated in some way across the band but due to lack of knowledge of such correlations a covariance matrix of radiance errors was constructed which assumes no correlation is present. This gives a conservative estimate of the resulting uncertainty. For a systematic error in line strength we have assumed a value of 1 % based on *Pickett et al.* [*1992*] which is probably a conservative estimate of the line strength error. Again, a covariance matrix of radiance errors due to this source was constructed which assumes that the errors are fully correlated across the band and with height. The resulting uncertainties in H_2O due to these three sources were combined by taking the root-sum-square uncertainty.

Field of view (FOV) direction: errors in the FOV direction are related to possible errors in misalignment of the 183 GHz radiometer FOV with respect to the 63 GHz FOV. Post launch calibration data from scans of the moon indicate a need for an alignment adjustment of the 183 GHz radiometer FOV from the pre-launch data (see *Jarnot et al., 1994*). The MLS Version 3 data used a misalignment value of 0.006 degrees which is somewhat less than the result of the studies based on moon-views of 0.011 degrees. We have assumed an uncertainty of 0.007 degrees in FOV direction (this is the uncertainty assumed in the MLS Version 3 data) and mapped this uncertainty into H_2O mixing ratio.

The following sources of systematic error were also considered but the resulting uncertainties in mixing ratio are generally not as significant as those which arise from the above-mentioned sources. The uncertainties in mixing ratio from the sources below are not plotted but have been included in the estimate of the root-sum-square systematic uncer-

tainty shown in Figure 13.

spectroscopy: errors in spectroscopic parameters can give rise to errors in retrieved mixing ratio. Line positions are known extremely accurately at microwave wavelengths and therefore do not represent a significant error source. Uncertainties in line strength have been included in the radiance scaling uncertainty mentioned above. Possible errors in linewidth were treated by assuming an uncertainty of 1.8 % in the broadening function and an uncertainty of 4 % in the temperature exponent. These uncertainties were estimated by combining information from *Bauer et al., [1989]* and *Goyette and De Lucia, [1990].* We also include a related uncertainty from imperfect knowledge of the Doppler shift of the emitted radiation, produced by line of sight velocity effects. Atmospheric wind along the line of sight will be the dominant source of error since both the spacecraft and earth velocity components are reasonably well known. An uncertainty of 70 m/s in line of sight velocity was assumed. The root-sum-square uncertainty in H_2O mixing ratio due to these three error sources is generally less than 2 %, although an uncertainty of 4 % is produced at 0.46 hPa which is due to the uncertainty in line of sight velocity.

dry air continuum: the dry air continuum is a semi-empirical contribution which is derived from radiance data from the 205 GHz radiometer [see *Read et al., paper in preparation*]. Possible errors produced by imperfect knowledge of the dry air continuum are estimated by assuming that no dry air continuum is present in the forward model, and comparing the subsequent retrieved H_2O mixing ratios with a standard retrieval. This is a 'worst case' scenario. The rms error in mixing ratio is estimated by dividing the worst case error by 3. This error source is only significant in the lower stratosphere where an uncertainty of $\sim$ 1.5 % occurs at 46 hPa and an uncertainty somewhat less than % occurs at 22 hPa.

FOV shape and position: FOV shape and position errors of the 183 GHz radiometer have been transformed into errors in radiance [*Jarnot, personal communication, 1994*]. A 1σ error of' 0.5 K is assumed and a covariance matrix of radiance error due to this source was constructed assuming these errors to be fully correlated across the band. The resulting uncertainty in H_2O mixing ratio is generally less than 1 %.

filter shape: each frequency channel across the H_2O band of the 183 GHz radiometer has an associated filter shape and position. Filter position errors are negligible but errors in filter shape could give rise to worst case errors in calibrated radiance of $\sim 0.5\%$ [*Jarnot, personal communication, 1994*]. A covariance matrix of radiance error due to this source was constructed with no correlations between channels. The resulting uncertainty in H_2O mixing ratio is negligible compared to the other systematic uncertainties mentioned above.

Finally, we give an estimate of the total uncertainty in MLS H_2O derived from the estimated uncertainties, both random and systematic, mentioned above. We also include the smoothing error [*Marks and Rodgers, 1993*] which represents the contribution of the *a priori* errors to the retrieved uncertainty. Figure 14 shows the estimated precision (from method 3 above), the root-sum-square (rss) systematic uncertainty and the smoothing error along with the root-sum-square of these three uncertainties. In section § 7 we give a summary table of the estimated precision (from method 3 above) and accuracy (rss error in Figure 14) for the useful vertical range of MLS Version 31120 data.

5. Comparison of MLS and correlative measurements

We now compare MLS H_2O data with measurements from four other observing systems. Two of these, a frost-point hygrometer and an infrared spectrometer are balloon-mounted.

The other two are a ground-based microwave spectrometer and a satellite-borne instrument which measures infrared absorption during solar occultations.

5.1 Frost point hygrometer data.

This instrument has an altitude range from the ground to ~28 km with a vertical resolution of 250 m. The accuracy of these measurements is 10 %; their precision is 10 % in the stratosphere [11?/]) *s, person* (11 *communications, 1992*]. The measurement sites which have have been used in this MLS-correlative comparison are: Boulder (40.0°N, 105.00\V)," Hilo, Hawaii (19.7°N, 204.9°E), and Lauder, New Zealand (45.00s, 109.4°E). Data were also taken during the Central Equatorial Pacific Experiment (CEPEX) at approximately (2.0°N, 157.5°W).

We have used the 12 balloon profiles distributed over these sites, for which there was coincident MLS water vapour data. 1"igure15 shows a typical profile, taken in this case at Hilo. Some of the closest MLS profiles are shown for comparison. The two data sets overlap over a restricted height range; the balloon data and the MLS data can be usefully compared at the 22 and 46 hPa levels. We tll(>l('fore calculated the differences between each balloon profile and the nearest MLS profile at these levels. At 46 hPa, the mean difference (MLS-balloon), taken over these 12 comparisons, is 0.2 ppmv, while the root mean square difference is 0.5 ppmv. At 22 hPa, the mean difference is 0.1 ppmv and the rms difference is 0.4 ppmv, the average being taken over the 6 balloon flights which reached a sufficient altitude for a comparison to be made at this level. We conclude that the systematic bias between the two data sets is smaller than 0.2 ppmv and that the random differences are within the quoted uncertainties. We note that none of the profiles used are at a latitude

poleward of 45°.

5.2 Ground-based microwave data.

This instrument is a ground-based water vapour milli meter wave spectrometer. All measurements used in this comparison have a vertical range between 30 and 80 km. The total absolute error of these measurements is $\sim$ 10 % over the height range 40-70 km [*Nedoluha et al., 1995*]. This technique has a vertical resolution of $\sim$15 km. This is considerably coarser than the resolution of MLS, so for a better comparison it would be desirable to smooth the MLS data using the averaging kernels of the ground-based instrument. We have not done this so it should be borne in mind that MLS may detect features in the atmosphere which the ground-based instrument cannot resolve. The measurement site is Table Mountain Observatory (TMO), situated at 34.4°N, 243.0°E, the data is a daily average and is provided with a pressure grid, the conversion from height to pressure having been performed using temperature and pressure fields from the National Meteorological Center (NMC) and the Middle Atmosphere Program (MAP) model [*Hedin, 1991*].

h41,S Version 3 data are compared with Version 2 of the ground-based data in Figure 16, where we plot both the mean difference (MLS – ground-based) and the rms difference. Data used in the comparison are from the period of 23rd January 1992 to 13th October 1992; this period provided a total of 186 days on whit.]1 both MLS and ground-based measurements were available. The rms difference is not much greater than the mean difference, suggesting that much of the difference between the two data sets is systematic. The ground-based data is less accurate at lower altitudes; some of the difference at 2.2 hPa and perhaps 1.0 hPa may be attributed to this. The MLS Version 3 values at 0.46 and 0.22 hPa are probably too

large by about 1 ppmv. The MLS Version 3 value at ().1 Ill)a is often as great as 10 ppmv. This is thought to be an artifact of the retrieval which we hope to remove in subsequent versions of the processing software. It is for this reason that we recommend that data from ().1 hPa and above should not be used for scientific purposes.

5.3 FIRS-2 data.

This instrument is an i]lfra-reel emission Fourier transform spectrometer carried by a balloon [*Johnson et al. 1994*]. Its vertical range is approximately 100- 3 h Pa, with a sampling interval of approximately 4 km, conveniently filling in the gap between the frost-point hygrometer and ground-based microwave data sets. It made three flights during the period when the 183 GIIz radiometer of MLS was operational, at times and places chosen to coincide with UARS lillll)-view'i llglllc:as~l lcl~lrllts. Figure 17 shows a FIRS-2 profile and an MLS profile. As with the frost-point hygrometer data, the profiles agree well in the lower stratosphere. Furthermore, the MLS profile becomes greater than the FIRS-2 profile as height increases, suggesting that the difference between the ground-based microwave data and MLS data is largely because MLS data are too high, rather than because the ground-based values are too low. These features are repeated in the other two 1"11{S-2 flights.

The MLS Version 3 software cannot retrieve water vapour at 1 ()() hPa. The values it produces are almost entirely climatological, but it is worth remarking that they are always too high when compared with correlative data. It will be possible, by using a nonlinear retrieval, to measure water vapour at this level; the comparison with correlative data suggests that a revised climatology is desirable before this is attempted. It is planned that future versions of the software will use a climatology which incorporates the SAGE II

data set [*Rind et al. 1993*].

5.4 Halogen Occultation Experiment (HALOE) data

In this section we present a comparison of MLS Version 3 H_2O data with Version 17 H_2O data from the HALOE instrument which is also onboard UARS. The Halogen Occultation Experiment (HALOE) is a limb sounding instrument which measures atmospheric absorption of solar infrared radiation during sunrise and sunset events. The characteristics of the UARS orbit and the solar occultation combine to produce a coverage pattern giving 15 sunrise profiles at one particular latitude and 15 sunset profiles at a different latitude on each day! These profiles are spaced $\sim 24^{\circ}$ apart in longitude with the latitude coverage changing throughout the year [*Russell at al., 1993*]. HALOE is capable in clear air of measuring profiles from $\sim$ 0.01 hPa to cloud top, i.e. the tropopause or lower. The overall accuracy of the HALOE Version 17 H_2O profiles is estimated to be 20-25 % in the lower stratosphere, 10-15 % in the upper stratosphere and 15-20 % in the lower mesosphere. The vertical resolution of the HALOE profiles is ~ 2 km.

The differing coverage patterns of the MLS and HALOE instruments limit the latitudinal range and temporal extent of the comparison. During periods when the coverage patterns overlap, MLS data is used to build a representation of the way in which HALOE samples the atmosphere. These periods are normally around 20 days in duration. For each day within one of these periods, the average latitude of the HALOE profiles was calculated. Then, for the ascending and descending orbit modes of MLS, the profiles enveloping this average HALOE latitude were found. The corresponding MLS profile, for each orbit, at the average HALOE latitude was then obtained by linear interpolation. The zonal mean difference

between the MLS profiles and the HALOE profiles (MLS- HALOE) was then calculated for each day of the comparison.

Figure 18 shows a contour plot of this zonal mean difference for the period 21st January 993 to 8th February 1993. The latitudinal coverage for this comparison period is from 30°N at the beginning of the period to 50°S at the end of the period. The zonal mean difference is expressed in units of ppmv. The comparison in Figure 18 uses MLS data from ascending orbit tracks only, however, similar features are produced when using data from descending orbit tracks. The results of this particular comparison are typical of those from other periods which have been studied.

In general, the zonal mean differences do not show any strong variation with latitude. In the lower stratosphere MLS and HALOE H_2O values differ by less than 0.5 ppmv (10 %) with MLS values tending to be larger than HALOE values. At 46 hPa the MLS values can be slightly less than those of HALOE. These differences are comparable with the H_2O error estimate produced by the MLS retrieval algorithms for this region of the atmosphere. In the upper stratosphere and lower mesosphere MLS H_2C values are consistently higher than the HALOE values by 1.0- 1.5 ppmv (1020 %). These differences tend to be greater than the MLS error estimate and are also consistent with comparisons with other correlative measurements presented earlier in this section. At 0.1 hPa the MLS H_2O values can be as much as 3 ppmv (30 %) larger than the HALOE values. At this pressure level the MLS Version 3 H_2O values are considered to be unphysically large (see section § 6).

6. Topics for Future Work

While the Version 3 water vapour is a useful quantity there are some problems associated

with t and improvements which can be made. Recent research [*Liebe et al., 1992*] has shown that the oxygen lines used to retrieve temperature and pressure have a slightly smaller linewidth than was assumed in the Version 3 software. Tests show that using the corrected linewidths gives somewhat lower values for water vapour in the stratosphere. The decrease is less than 0.2 ppmv in the lower stratosphere, and is typically 0.3- 0.5 ppmv in the upper stratosphere and tends, therefore, to bring the MLS water vapour into better agreement with the correlative measurements. Also, using the new oxygen linewidths gives rise to smaller discrepancies between measured and calculated radiances.

A serious problem is the loss of information which occurs at 46 and 22 hPa in the winter at polar latitudes. The information is lost because the Version 3 software does not use radiances which come from ray paths which are judged to be optically thick. These radiances are related nonlinearly to the water vapour content so a nonlinear retrieval process would be required to make full use of them. Tests have suggested that the criterion used in Version 3 is rather stricter than necessary and that using a few more radiances than are used at present would make the retrieval better rather than worse. This cannot be implemented immediately because it causes other problems, particularly with the baseline.

The same tests suggest that a similar problem is at least partly responsible for the notch at 0.1 hPa. The center channel, channel 8, becomes optically thick and is not used at this level while channels 7 and 9 only have sufficient signal to retrieve water vapour below this level.

With these changes, a future linear retrieval should be an improvement on the current version. However, to extract full information from the measurements will require a non-linear retrieval. Initial tests show that it is possible to retrieve water vapour at 100 hPa by this

technique. It is also possible [*Read et al. 1994*] to retrieve upper tropospheric water vapour rom MLS band 3 (at 206 GHz) , normally used for stratospheric chlorine monoxide. We plan to include this information along with that from the 183 GHz radiometer into a single etrieval process, producing a measurement of water vapour from the upper troposphere to the mesosphere.

In addition to these major changes, there are some minor artefacts in the data which we plan to eliminate. There are occasional profiles for which the retrieval has clearly failed, but which are not flagged as being bad. One known cause occurs during the generation of calibrated radiances (Level 1 data) and will be eliminated in future versions of the software. Another artefact occurs in the data at 22111'a which show a small systematic dependence on the UARS yaw cycle. This effect is not fully understood at present, but is clearly an artefact which needs to be removed. An important improvement will be the use of a revised climatology; the current version is supplying unsuitable *a priori* values at 100 hPa. Finally, tracer transport studies [*Mancy et al., 1994*] suggest that MLS water vapour in the upper stratosphere does not behave like a passive tracer. We aim to establish whether this is an artefact of the retrim'al or the tracer transport code, or whether it is a real physical effect.

7. Estimated Accuracy and Precision of MLS Version 3 Data

MLS Version 3 H_2O retrievals give reasonable values in the stratosphere, but consistently overestimate other correlative measurements. The current range of useful sensitivity (as measured by the data quality see section § 4) is between 46 hPa and 0.0 hPa, although lower mesospheric retrievals appear suspect at present due to a 'notch' around ~ 0.1 hPa (see section § 6). Retrievals at 46 hPa in the polar winter can have poor data quality (see

section § 2). Therefore, the recommended pressure range for scientific studies using MLS $1\,1_2O$ is from 22 hPa to ().2111'a for all latitudes, and from 46111'a to 0.2 hPa at the tropics and mid-latitudes.

Comparison with other $1\,1_2O$ measurements suggests that MLS $1\,1_2O$ values are too high by $\sim 5\%$ at 46 hPa and at 22 hPa and by 15 20 % in the range 1 hPa to 0.22 hPa.

The characteristics of MLS $}1_2O$ 183 GIIz measurements retrieved using Version 3 of the software are summarised in Table 1. The precision estimates in Table 1 may be slightly pessimistic as they are based on the observed variability of retrieved profiles in the tropics and may contain effects of atmospheric variability. The estimates of accuracy in Table 1 contain the effects of systematic uncertainties, the contribution of the *a priori* error to the retrieved uncertainty and the above-mentioned precision estimates. 111 the pressure rail'gc 1 hPa to ().221]1'a, the estimated accuracy in Table 1 does not fully account, for the differences found in the comparisons with correlative data. This suggests that some systematic effects may not be accounted for in the error analysis of section § 4.

Acknowledgm[71 1.s. We thank many colleagues, at Edinburgh University, Heriot-Watt University and the Rutherford Appleton Laboratory in the United Kingdom and at the Jet Propulsion Laboratory in the USA, who have contributed to the MLS project. We are indebted to various persons from the UARS Project and elsewhere for the compilation of data and model values which make up the "UARS Climatology File", which is used as *a priori* information in the MLS retrieval process; in particular, we acknowledge the efforts of R. Seals and P. Connell. We also thank M. Allen for the default model profiles used as part of this procedure. Early simulations of MLS retrievals also benefited from the availability

of 3-D model results, made possible by W.L. Grose, G. Lingenfelser, and others at the NASA Langley Research Centre. We thank the groups at NOAA Climate Monitoring and Diagnostics Laboratory, the Naval Research Laboratory, Harvard-Smithsonian Centre for Astrophysics and NASA Langley Research Centre for kindly providing correlative data sets. The work in the UK was funded by SERC and NERC, and in the USA by NASA.

References

Backus, G.E., and J.F. Gilbert, Uniqueness in the inversion of inaccurate gross Earth data, *Philos. Trans. R. Soc. London, Ser. A266*, 123- 192, 1 97(1.

Barath, F.'J'., M.C. Chavez, R.E. Cofield, 1). A. 11'lower, M.A. Frerking, M.B. Gram, W.M. Harris, J.R. Holden, R.F. Jarnot, W .G. Kloczeman, G.J. Klose, G.K. Lau, M.S. Loo, B.J. Maddison, 1{..1. Mattauch, R.P. McKinney, G.E. Peckham, H. M. Pickett, G. Siebes, F.S. Soltis, R. A. Suttie, J. A. Tarsala, J.W. Waters, and W.J. Wilson, The Upper Atmosphere Research Satellite Microwave Limb Sounder instrument *J. Geophys. Res.98*, 1)6, 10,751-10,762, 1993.

Bauer, A., M. G odon, h 4 . Kheddar, and J.M. Hartmann, Temperature and perturber dependences of water vapor line-broadening. Experiments at 183 GHz; calculations below 1000" GHz, *J. Quant. Spectrosc. Radiat. Transfer 41*, No. 1, 49-54, 1989.

Bevilacqua, R. M., W.,]. Wilson, W.B. Ricketts, P.R. Schwartz, and R. J. Howard, Possible seasonal variability of mesospheric water vapor, *Geophys. Res. Lett. 12*, 397-- 400," 1985.

Bevilacqua, R.M., W..]. Wilson, and 1'.1{. Schwartz, Measurements of mesospheric water vapor in 19S4 and 1985: results and implications for middle atmospheric transport, ,1. *Geophys. Res. 92, 1*)6, 6679–6690, 1987.

Fishbein, E.F., W.G. Read, L. Froidevaux, and J.W. Waters, Validation of temperature and pressure measurements by the Upper Atmosphere Research Satellite Microwave Limb Sounder, *J. Geophys. Res.*, submitted, 1994.

Froidevaux, L., W. G. Read, T. A. Lungu, R.E. Cofield, E.F. Fishbein, D. A. Flower, R.F. Jarnot, B.P. Ridenoure, Z. Shippony, J.W. Waters, J.J. Margitan, H.S. McDermid, R. A. Stachnik, G.E. Peckham, G. Braathen, J. Deshler, J. Fishman, D. J. Hofmann, and S.J. Oltmans, Validation of UARS MLS ozone measurements, *J. Geophys. Res.*, submitted, 1994.

Goyette, T.M. and F.C. De Lucia, The pressure broadening of the $3_{1,3}$- $2_{2,0}$ transition of water between 80 K and 600"1<, *J. Mol. Spectroscopy 143*, No. 2, 346--358, 1990.

Hedin, A.E., Extension of the MSIS thermosphere model into the middle and lower atmosphere, *J. Geophys. Res. 96*, A2, 1159-1172, 1991.

Jarnot, R.F., R.E. Cofield, G.E. Peckham, and J .W. Waters, Calibration of UARS MLS, *J. Geophys. Res.*, submitted, 1994.

Johnson, D.G., K.W. Jucks, W.A. Traub and K.V. Chance, The Smithsonian stratospheric far-infrared spectrometer and data reduction system, J .G. R., in press, (1994).

Liebe, H.J., P.W. Rosenkranz, and G.A. Hufford, Atmospheric 60 GHz oxygen spectrum: new laboratory measurements and line parameters, *J. Quant. Spectrosc. Radiat. Transfer 48*, 629-643, 1992.

Manney, G.L., W.A. Lahoz, R.S. Harwood, R.W. Zurek , J. B. Kumer, J.L. Mergenthaler, A.E. Roche, A. O 'Neill, R. Swinbank, J.W. Waters, Lagrangian transport calculations using UARS data. Part 1: Passive tracers, *J. Atmos. Sci.*, submitted, 1994.

MA P, J.J. Barnett, and M. Corney, Handbook for Middle Atmosphere Program (MA}))> SCOSTEP Secretariat, University of Illinois, Urbana, USA, 1989.

Marks, C.J., and C.D. Rodgers, A retrieval method for atmospheric composition from limb emission measurements, *J. Geophys. Res. 98*, D8, 14,939- 14,953, 1993.

Nedoluh a, G.E., R. M. Bevilacqua, R. M. Gomez, 1).1,. Thacker, W.B. Waltman, and 'J'. A. Pauls, Ground-based measurements of water vapor in the middle atmosphere, *J. Geophys. Res. 100*, 1)2, 1995.

Pickett, H. M., R.L. Poynter, and E.A. Cohen, Submillimeter, millimeter and microwave spectral line catalog, Technical report 8023, Revision 3, Jet 1'ropulsion 1.aboratory, 1992.

Read, W.G., J.W. Waters, L. Froidevaux, 1). A. Flower, R.F. Jarnot, D.L. Hartmann, 1{. S. Harwood, and R.B . Rood, Upper tropospheric water vapor from UARS MLS, *Bull. A mer. Met. Soc.*, submitted, 1994.

Reber, C. A., The Upper Atmosphere Research Satellite *Trans. Am. Geophys. Un.* 7 1, No. 51, 1,867-1,868, 1,873-1,874,1,878,1990.

Remsberg, E.E., J.M. Russell 111, and C.-Y. Wu, An interim reference model for the variability of the middle atmosphere water vapor distribution, *Adv. Space Res. 10*, 51 - 64, 1990.

Rind, 1)., E.-W. Chiou, W. Chu, S. Oltmans, J. Lerner, J. Larsen, M. 1'. McCormick, L. McMaster, ovm-view of the Stratospheric Aerosol and Gas Experiment 11 Water Vapour Observations: Method, Validations and 1)ata Characteristics, *J. Geophys. Res. 98*, 1)3, 4835–4856, 1993.

Rodgers, (.I)., Retrieval of atmospheric temperature and composition from remote measuremer its of thermal radiation, *Rev Geophys. and Space Phys. 14*, 609- 624, 1976.

Rodgers, C.D., Characterization and error analysis of profiles retrieved from remote sounding measurements, *J. Geophys. Res. 95*, D5, 5587--5595, 1990.

Russell 111, J. M., J.C. Gille, E.E. Remsberg, 1,.1,. Gordley, 1'.1,. Bailey, 11. Fischer, A. Gird, S. 1{. 1 Drayson, W.F.J. Evans, and J.E. Harries, Validation of water vapor results measured by the Limb Infrared Monitor of the Stratosphere (LIMS) experiment on NIMBUS 7, *J. Geophys. Res. 89*, D4, 5115 - 5124, 1984.

Russell 111, J.M., L.L. Gordley, J.]]. Park, S.R. Drayson, W.D. Hesketh, R.J. Cicerone, A.F. Tuck, J .E. Frederick, J.E. Harries, and P.J. Crutzen, The Halogen occultation Experiment, *J. Geophys. Res. 98*, D6, 10,777–10,797, 1993.

Tsou, J- J., J ..), Olivero, and C.L. Croskey, Study of variability of mesospheric 11_20 during spring 1 984 by gmuI]cl-based microwave radiometric observations, *J. Geophys. lies. 93*, 1)5, 5255-5266, **1988**.

Waters, J .W., Absorption and emission by atmospheric gases, in *Methods of Experimental Physics, 12B*, (l,. Meeks, d.), 142-176, Academic Press, New York, 1976.

Waters, J.W., Microwave Limb Sounding, in *Atmospheric Remote Sensing by Microwave Radiometry*, (M .A. Janssen, ed.), ch. 8, John Wiley & Sons, New York, 1993.

Waters, J .W., W. G. Read, L. Froidevaux, T. Lungu, V.S. Perun, R.A. Stachnik, R.F. Jarnot, R.E. Cofield, E.F. Fishbein, D. A. Flower, J.R. Burke, J.C. Hardy, L.L. Nakamura, B.P. Ridenoure, Z. Shippony, R.P. Thurstans, 1.. M. Avallone, D. W. Toohey, R.L. deZafra, and 1).'1'. Shindell, Validation of UARS MLS ClO measurements, J. *Geophys. Res.*, submitted, 1994.

Figure Captions

Fig. 1: Calculated limb emission in the spectral region 182-187 GHz which includes both spectral sidebands of MLS band 5 (vertical dashed lines) and band 6 (vertical dotted lines). The position of the 183 GHz radiometer local oscillator (LO) at 184.78 GHz is indicated. Spectra for tangent pressures of 46 hPa and 4.6 hPa are plotted.

Fig. 2: MLS band 5 (183 GHz H_2O) limb radiance profiles for channels 1-8 for a tropical profile (4.25°N, 334.99°E) on 10th January 1992.

Fig. 3: MLS band 5 (183 GHz 11_20) radiance spectra for a tropical profile (4.25°N, 334.99°E) on 10th January 1992 at three tangent pressures: 0.11 hPa (top panel), 3.7 hPa (middle panel) and 50111'a (bottom panel).

Fig. 4: radiant.cs from channels 1 to 8 for a MLS scan at latitude 56.05°N, longitude 255.13°E on 10th January 1992. Also shown, by the thick line, is the MLS temperature profile, scaled by the 0.58 sideband ratio. Note that the baseline is about 2 1<; the radiances tend to this value as height increases.

Fig. 5: MLS band 5 radiance residual profiles for channels 1-15 for 10th January 1992 at (4.25°N, 334.99°E). The horizontal bars represent the 1σ measurement noise.

Fig. 6: MLS band 5 average radiance residual spectra for 10th January 1992 within latitude band 10°N-10°S. The pressure range is displayed above each panel. Vertical bars represent the standard error on the mean measured radiance. The number of limb views included in the calculation of the average radiance residual ranges from around 200 in the pressure

range 0.032- 0.01 hPa to around 800 in the pressure range 100- 31.6 hPa.

Fig. 7: MLS band 5 average radiance residual spectra for 10th January 1992 within latitude band 60°N- 80°N. The pressure range is displayed above each panel. Vertical bars represent the standard error on the mean measured radiance. The number of limb views included in the calculation of the average radiance residual ranges from around 200 in the pressure range 0.032- 0.01 hPa to around 800 in the pressure range 100- 31.6 hPa.

Fig 8: (a zonal mean of smoothed $_2$O field used to represent the true distribution i tests of retrieval closure, units are ppmv (field taken fron MLS Version 3 H_2O retrieval for 17th September 992) (b) zonal mean of retrieved H_2(using simulated radiances based on the true distribution, units are ppmv. (c) zonal mean difference (retrieval truth) H_2O, units are ppmv. (d) rms difference between etrieval and truth, units are ppmv

Fig. 9: Averaging kernels for M LS Version 3 H_2O retrievals.

Fig. 10: Vertical resolution of M LS Version 3 H_2O retrievals.

Fig. : Estimated random errors associated with the retrieval of MLS H_2O. The units are ppmv Line (1) is an estimate of precision given by method o section §4.

Fig. 12: Precision estimates for MLS Version 3 H_2O. Method 1: from formal error analysis, method 2: variability of retrieved profiles near to the orbit turning points i the summer hemisphere, method 3: variability of retrieved profiles in the tropics. The units are ppmv.

Fig 13: Estimated systematic uncertainties associated with the retrieval of MLS H_2O

Fig. 14: Estimated uncertainties associated with the retrieval of MLS H_2O. rss error: root-sum-square of precision, systematic error and smoothing error, precision (3): estimate of precision using method 3 (see text), rss systematic error: root-sum-square of estimated systematic errors, smoothing error: contribution of the *a priori* errors.

Fig. 15: A typical water vapour profile measured by a balloon mounted frost point hygrometer (solid line). The balloon was launched from a site in Hawaii at latitude 19.4°N, longitude 155°W, on 24 March 1991. Several MLS profiles for nearby locations are shown by dashed and dot-dash lines, their error bars are shown by dotted lines. The balloon profile is within the MLS errors at 46 and 22 hPa.

Fig. 16: Comparison of MLS Version 3 water vapour with the Version 2 data from the ground-based microwave instrument. Data are from the period of 23rd January 1992 to 13th October 1992; a total of 186 days for which both MLS and ground-based measurements were available. The left hand plot shows mean profiles; the solid line is MLS data, the dashed line ground-based. The right hand plot shows the mean difference, MLS - ground-based (solid) and the rms difference (dashed).

Fig. 17: Water vapour profiles measured by MLS (solid line) compared with FIRS 11 (squares) on 29 September 1992. The MLS profile is at latitude 37.5 °N, longitude 103.2 °W, the FIRS II profile is at latitude 36.9 °N, longitude 100.4 °W.

Fig. 18: Zonal mean difference (MLS -- HALOE) between MLS Version 3 H_2O and HALOE Version 17 H_2O for the period 21st January 1993 to 8th February 1993. The numbers along the top of the plot are the UARS day numbers for which each zonal mean difference profile

was calculated. This comparison period begins on UARS day 498 (2 s January 1993) where the la tude of coincident MLS and HALOE measurements is ~ 30°N and the eriod ends on JARS day 516 (8 .1 February 993) where the coincident latitude is 50°S The MLS data used is from ascending orbit tracks only. The zonal mean differences are expressed in units of ppmv.

W.A. ahoz, CGA Department o Meteorology, Reading University, ngland, UK RG6 2A

R.S. Harwood, W.A. ahoz, H.C. Pumphrey, M.R Suttie, Department of Meteorology, Edinburgh Jniversity, Scotland, K H9 3JZ

C.L.Lau, G.E. eckham, R A Suttie, Department of Physics, Heriot-Watt Jniversity, Scotland, UK EH14 4AS

. Froidevaux T.A. Lungu, W.G. Read, Z. Shippony, J.W. Waters, Jet Propulsion Laboratory, California Institute o Technology, asadena, CA, USA 91109

E C Nedoluha, Naval Research Laboratory, Code 7220 Washington, D JSA 20375

S . Oltmans, NOAA Climate Monitori ig and Diagnost cs Laboratory, Boulder, CO, USA 80303

J.M ussel NASA angley esearch Centre, Hampton VA, USA 23665

W.A Trau , arvard-Smithsonian Centre for Astrophysics, Cambridge, MA, U SA 02138

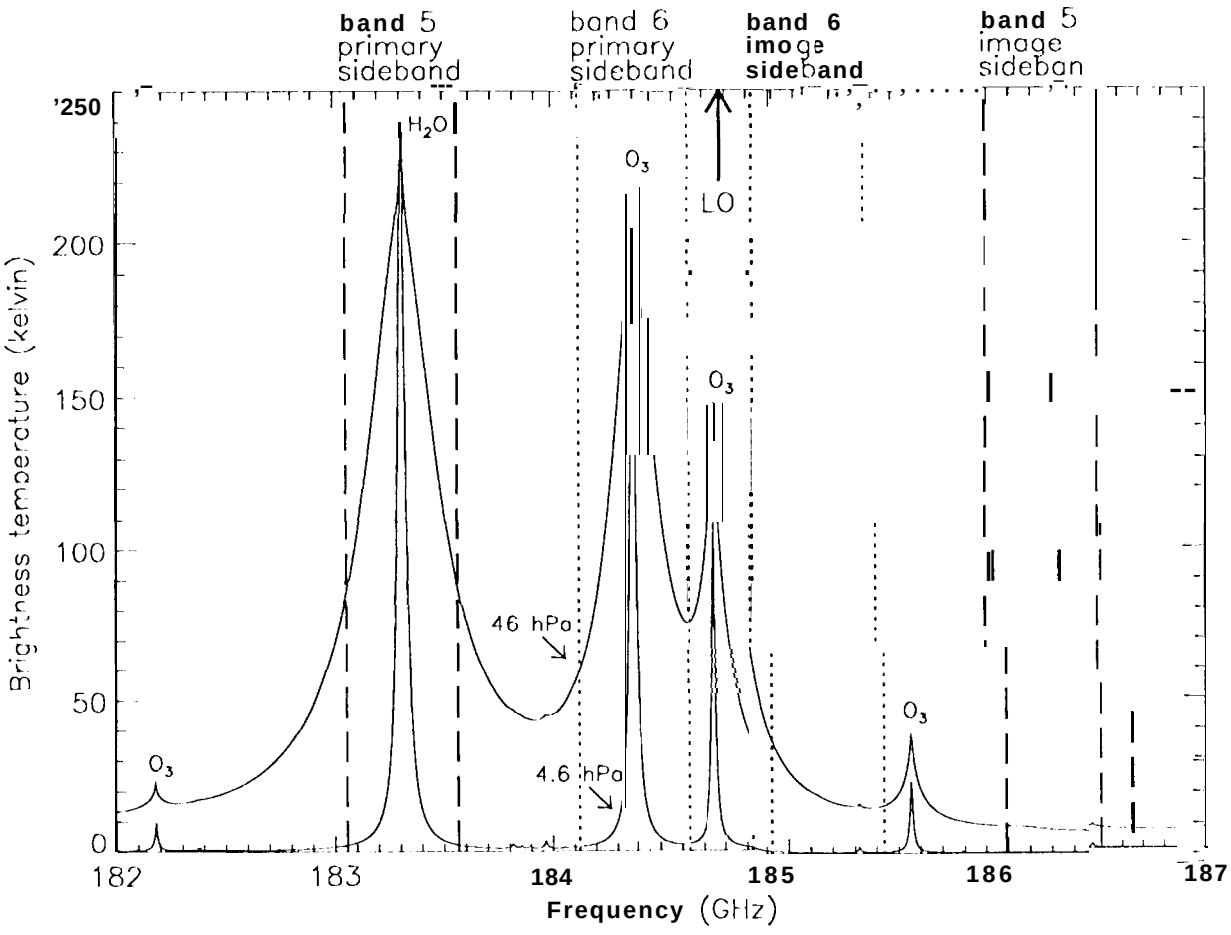
band 5
primary
sideband
band 6
primary
sideband
band 6
image
sideband
band 5
image
sideban
'250
200
150
100
50
0
Brightness temperature (kelvin)
H_2O
O_3
LO
O_3
46 hPa
O_3
O_3
4.6 hPa
182
183
184
185
186
187
Frequency (GHz)

Fig 1

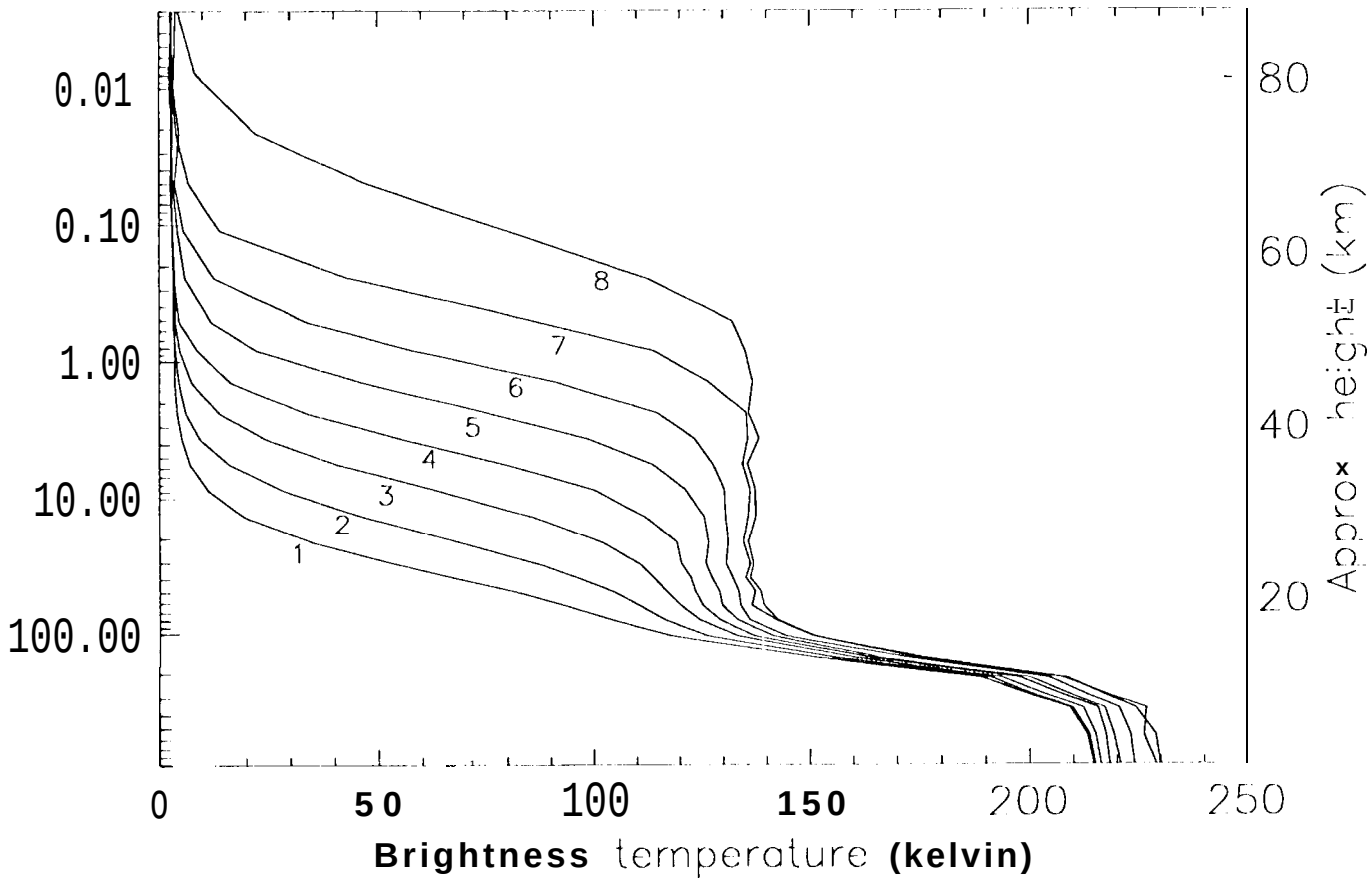
0.01
0.10
1.00
10.00
100.00
80
60
40
20
Approx height (km)
8
7
6
5
4
3
2
1
0
50
100
150
200
250
Brightness temperature (kelvin)

Fig 2

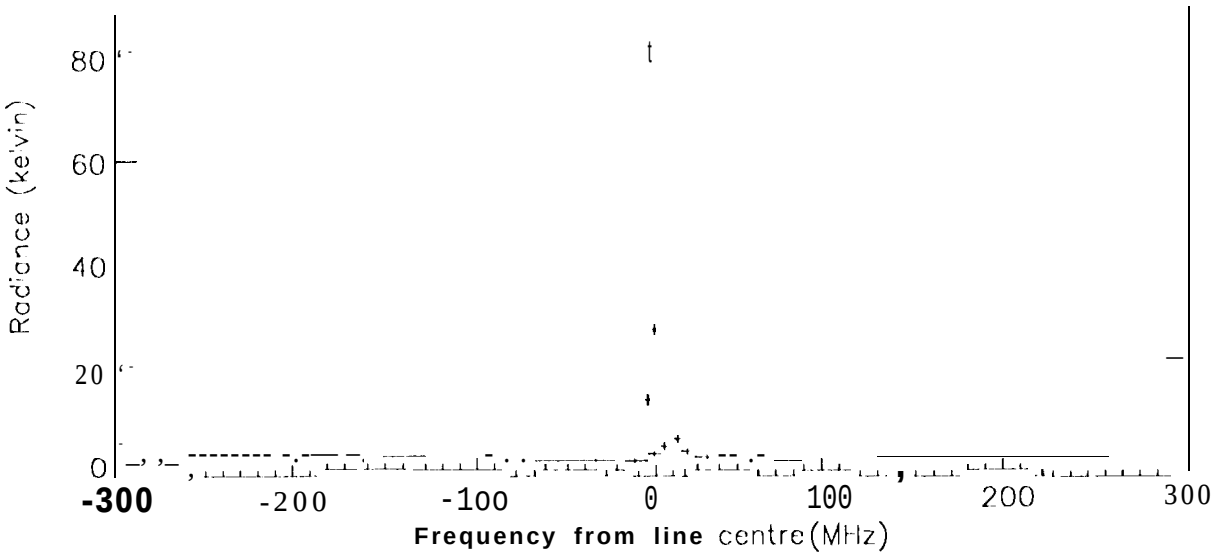
80
60
40
20
0
Radiance (kelvin)
-300
-200
-100
0
100
200
300
Frequency from line centre (MHz)

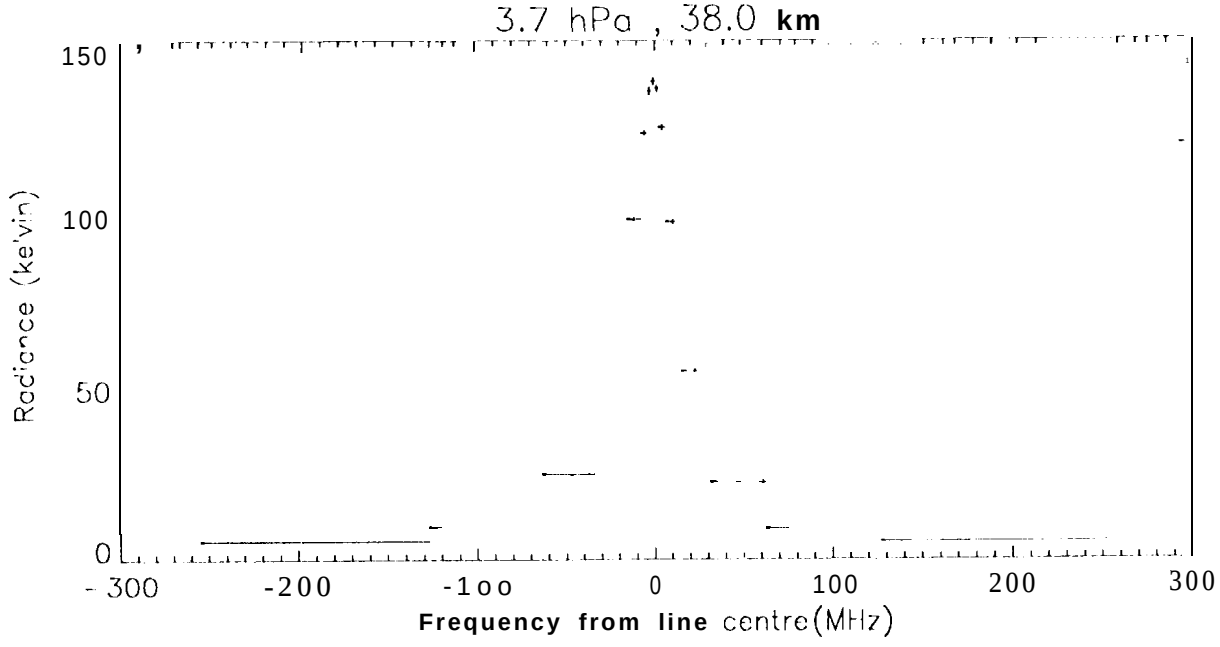
3.7 hPa , 38.0 km
150
100
50
0
Radiance (kelvin)
-300
-200
-100
0
100
200
300
Frequency from line centre (MHz)

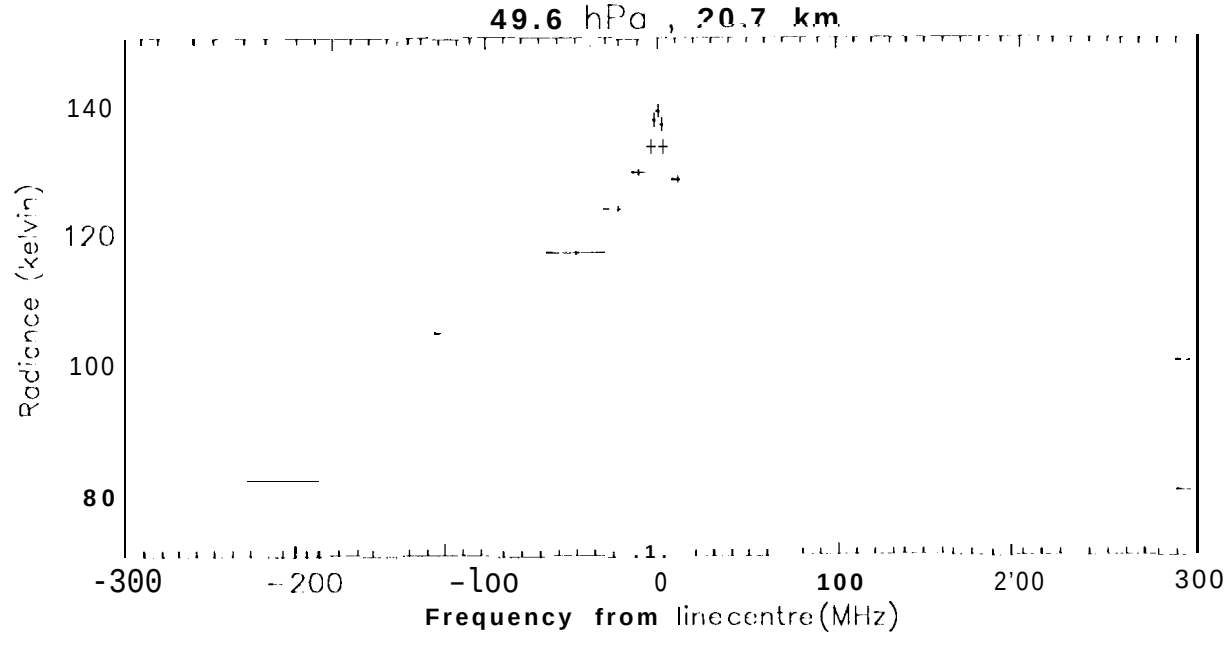
49.6 hPa , 20.7 km
140
120
100
80
Radiance (kelvin)
-300
-200
-100
0
100
200
300
Frequency from line centre (MHz)

Fig 3

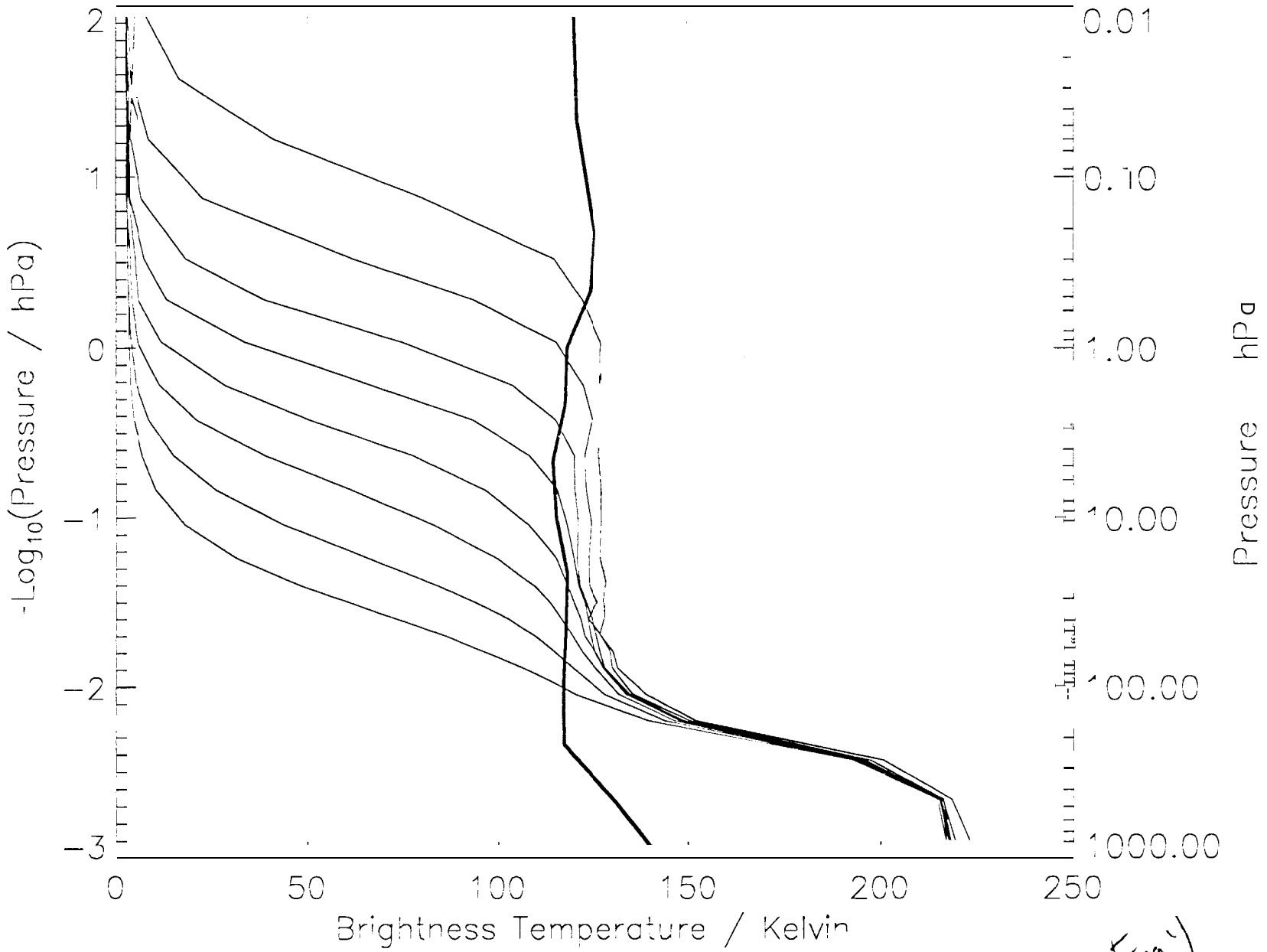
2
1
0
−1
−2
−3
-Log10(Pressure / hPa)
0
50
100
150
200
250
Brightness Temperature / Kelvin
0.01
0.10
1.00
10.00
100.00
1000.00
Pressure hPa

Fig 1

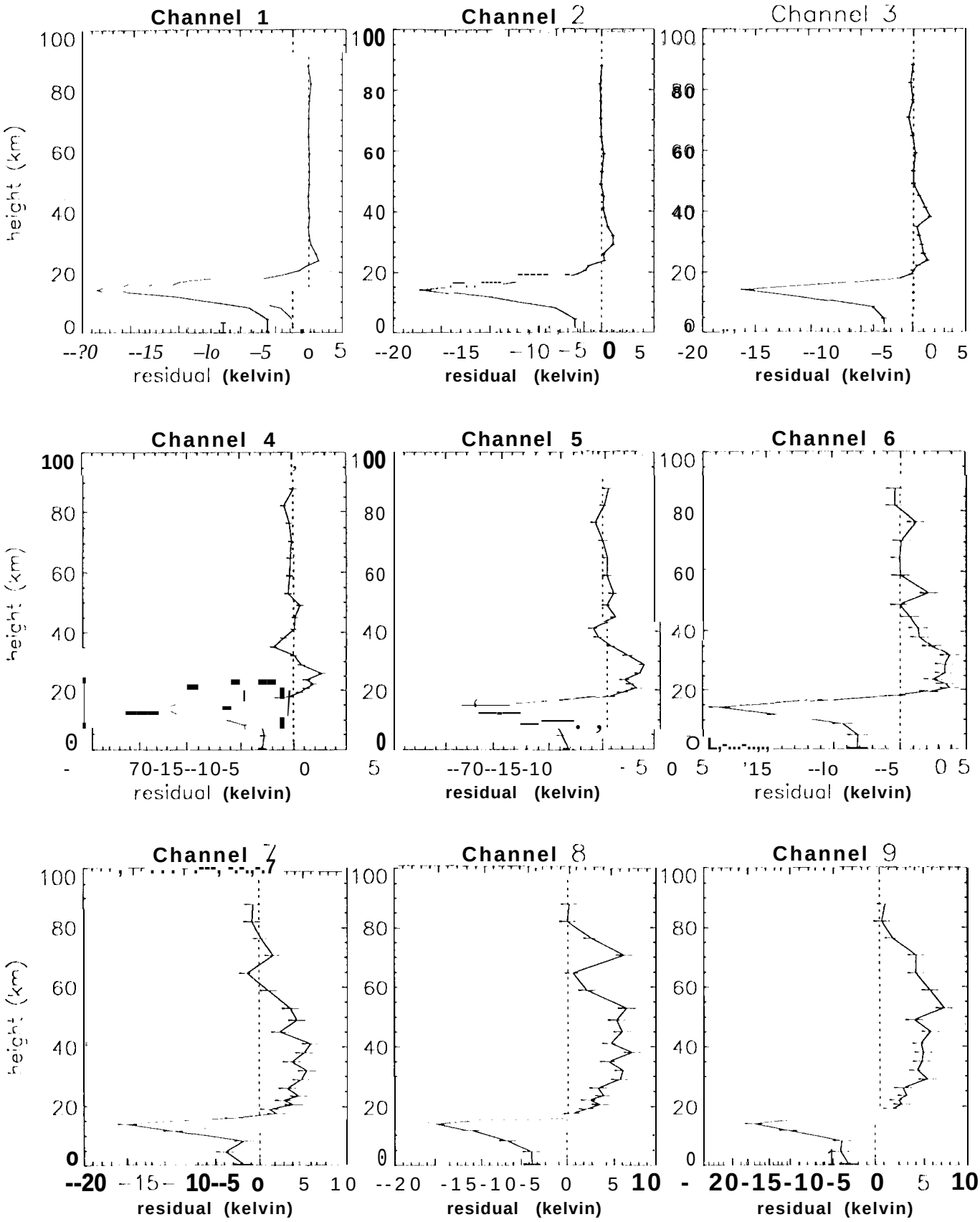
Channel 1
Channel 2
Channel 3
Channel 4
Channel 5
Channel 6
Channel 7
Channel 8
Channel 9
height (km)
residual (kelvin)

Fig 5

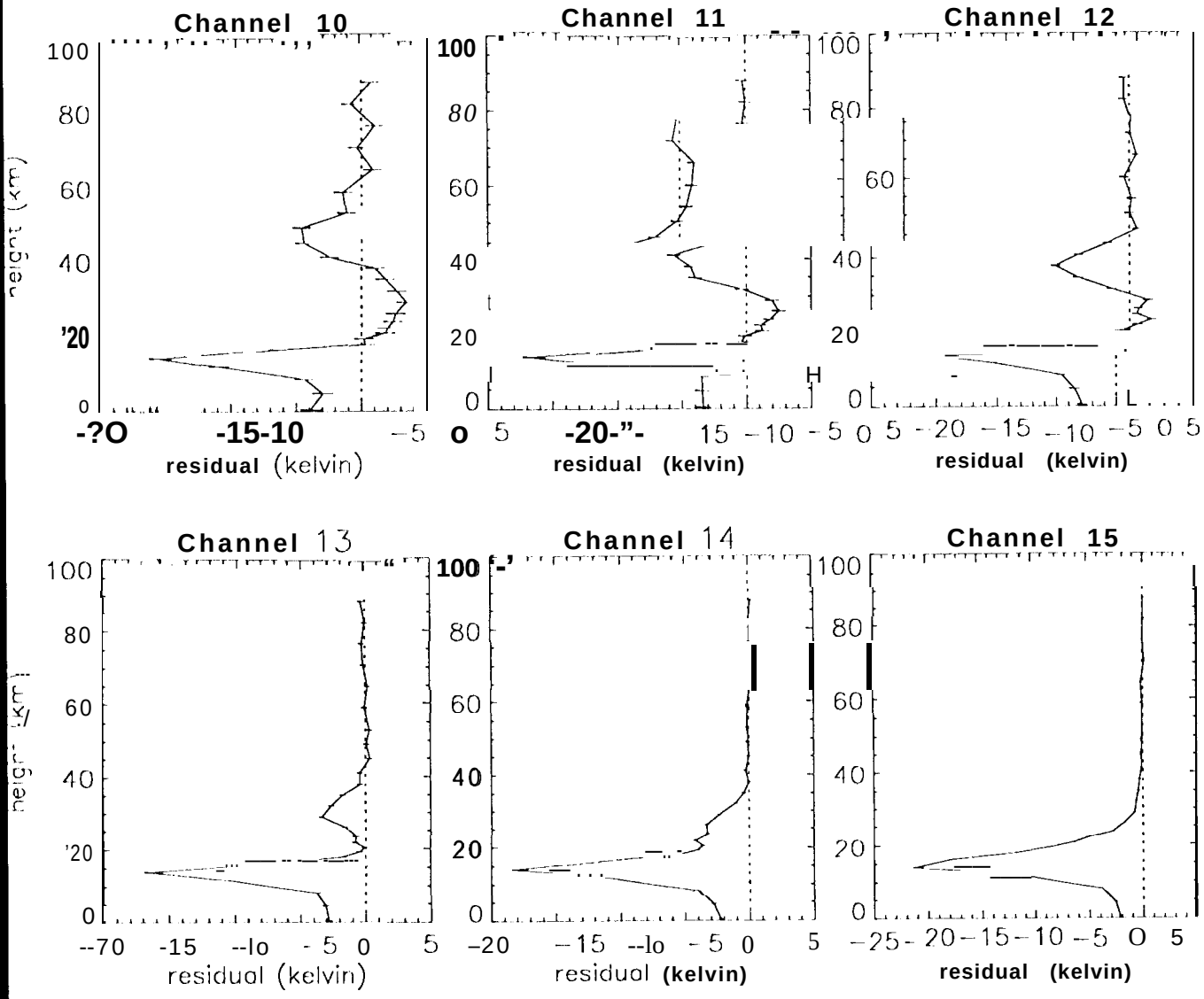
Channel 10
Channel 11
Channel 12
Channel 13
Channel 14
Channel 15
residual (kelvin)
residual (kelvin)
residual (kelvin)
residuol (kelvin)
residuol (kelvin)
residual (kelvin)

Fig 5

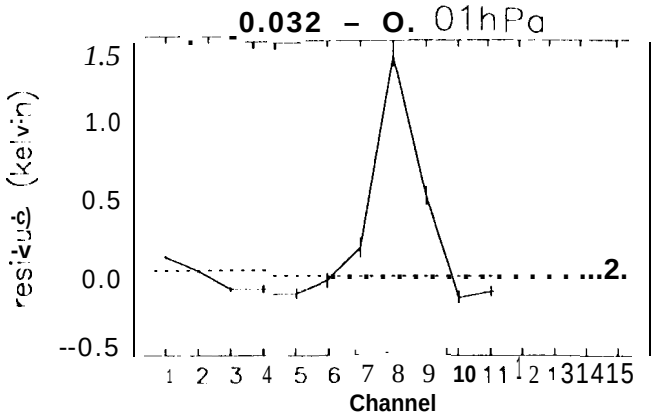
0.032 – O. 01hPa
residue (kelvin)
1.5
1.0
0.5
0.0
--0.5
1 2 3 4 5 6 7 8 9 10 11 12 13 14 15
Channel

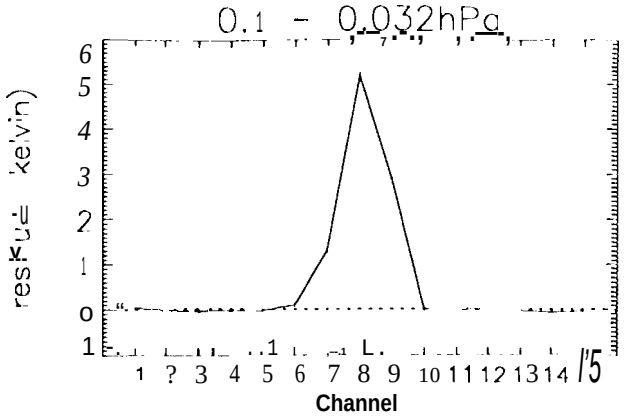
0.1 - 0.032hPa
residue (kelvin)
6
5
4
3
2
1
0
1 ? 3 4 5 6 7 8 9 10 11 12 13 14 15
Channel

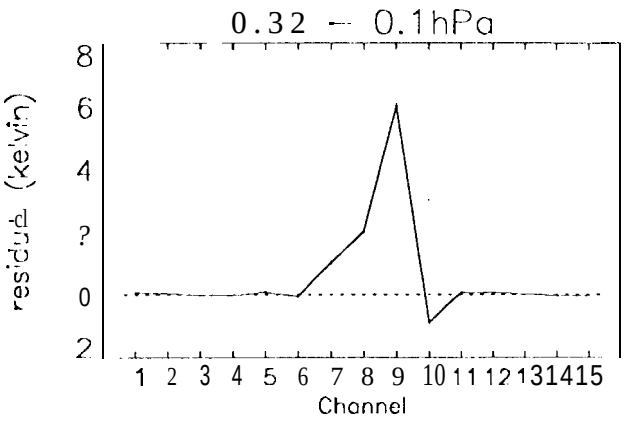
0.32 – 0.1hPa
residual (kelvin)
8
6
4
?
0
2
1 2 3 4 5 6 7 8 9 10 11 12 13 14 15
Channel

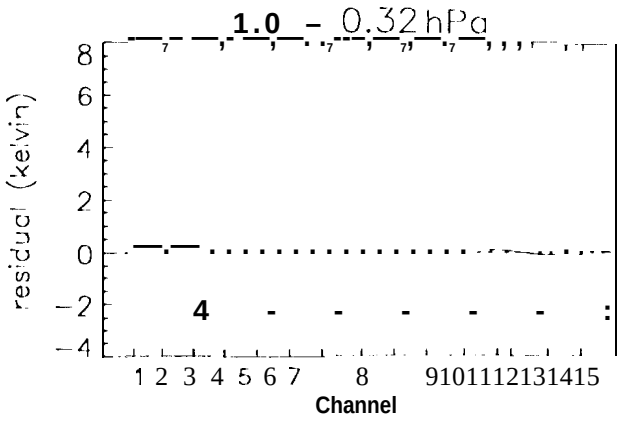
1.0 – 0.32hPa
residual (kelvin)
8
6
4
2
0
–2
–4
1 2 3 4 5 6 7 8 9 10 11 12 13 14 15
Channel

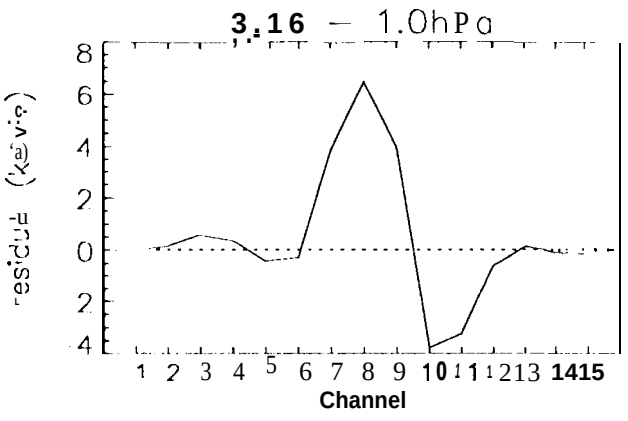
3.16 – 1.0hPa
residual (kelvin)
8
6
4
2
0
2
4
1 2 3 4 5 6 7 8 9 10 11 12 13 14 15
Channel

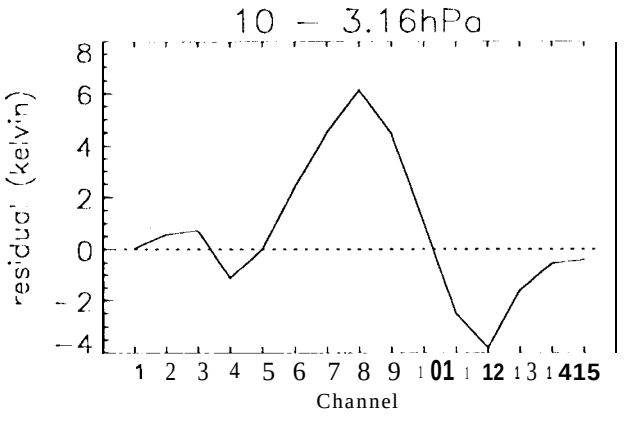
10 – 3.16hPa
residual (kelvin)
8
6
4
2
0
- 2
–4
1 2 3 4 5 6 7 8 9 10 11 12 13 14 15
Channel

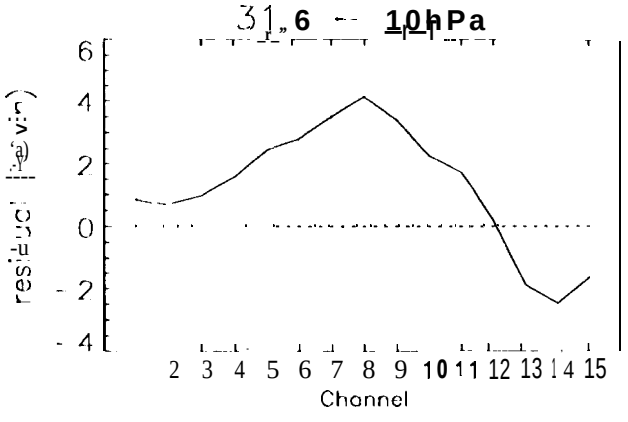
31.6 – 10hPa
residual (kelvin)
6
4
2
0
- 2
- 4
2 3 4 5 6 7 8 9 10 11 12 13 14 15
Channel

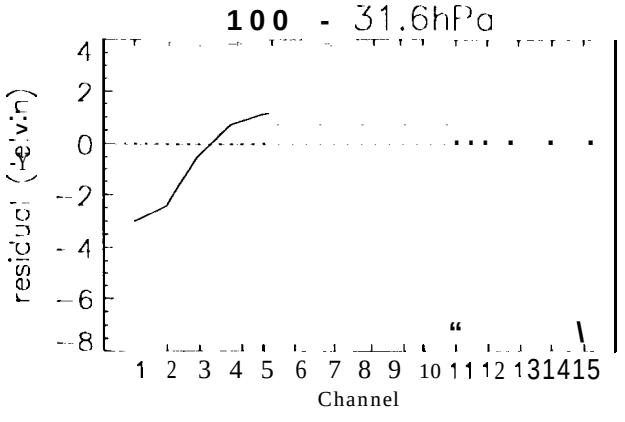
100 - 31.6hPa
residual (kelvin)
4
2
0
--2
- 4
–6
--8
1 2 3 4 5 6 7 8 9 10 11 12 13 14 15
Channel

Fig 6

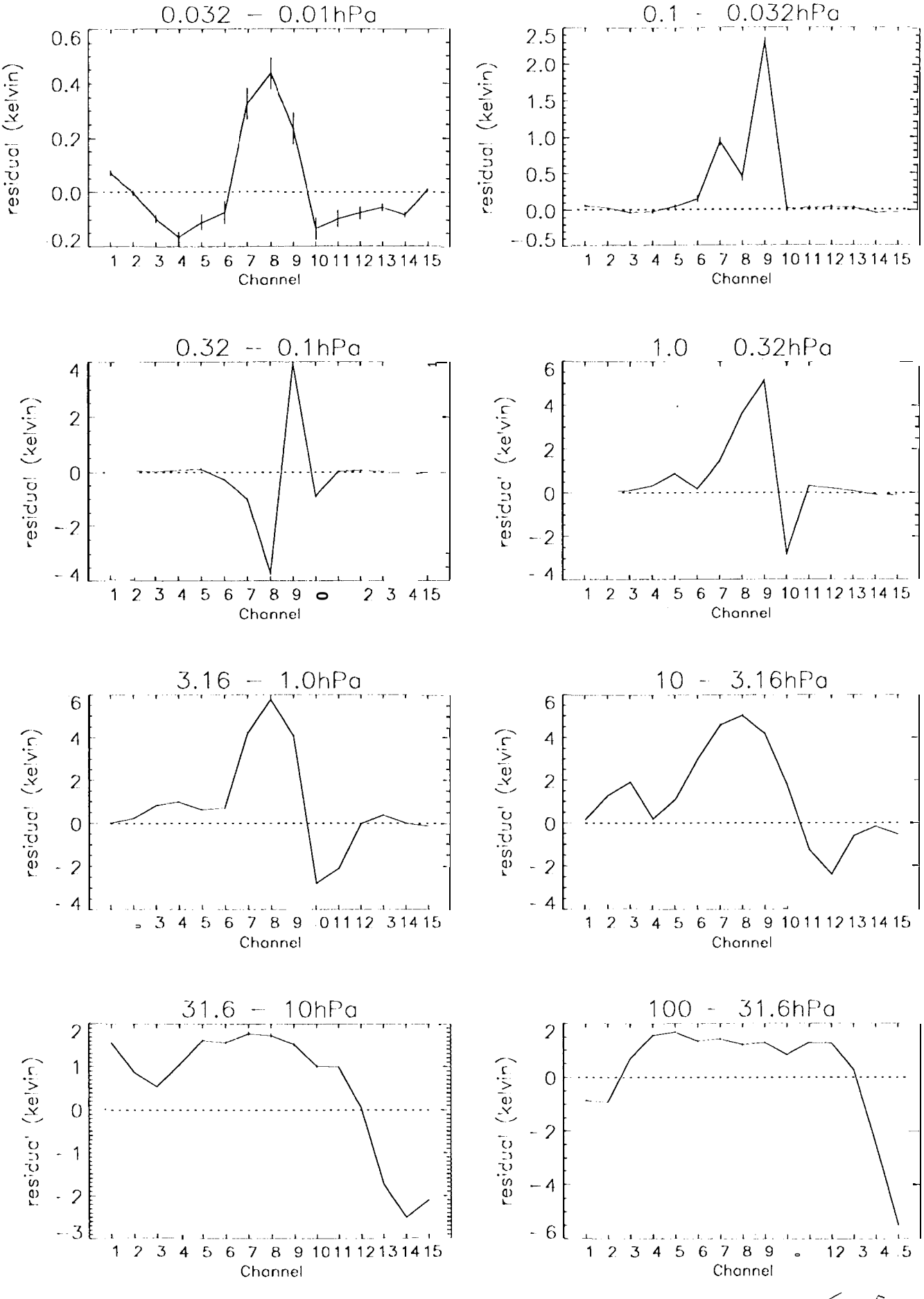
0.032 – 0.01hPa
0.1 - 0.032hPa
0.32 -- 0.1hPa
1.0 0.32hPa
3.16 – 1.0hPa
10 - 3.16hPa
31.6 – 10hPa
100 - 31.6hPa
residual (kelvin)
Channel

Fig 1

(b)
(c)
(c)
(d)
Pressure (hPa)
Pressure (hPa)
Pressure (hPa)
Pressure (hPa)
Latitude (degrees)
Latitude (degrees)
Latitude (degrees)
Latitude (degrees)
100.0
10.0
1.0
0.1
8.0
7.0
6.0
5.0
4.0
3.0
0.8
0.6
0.4
0.2
0.0
-0.2
-0.4
-80
-60
-40
-20
0
20

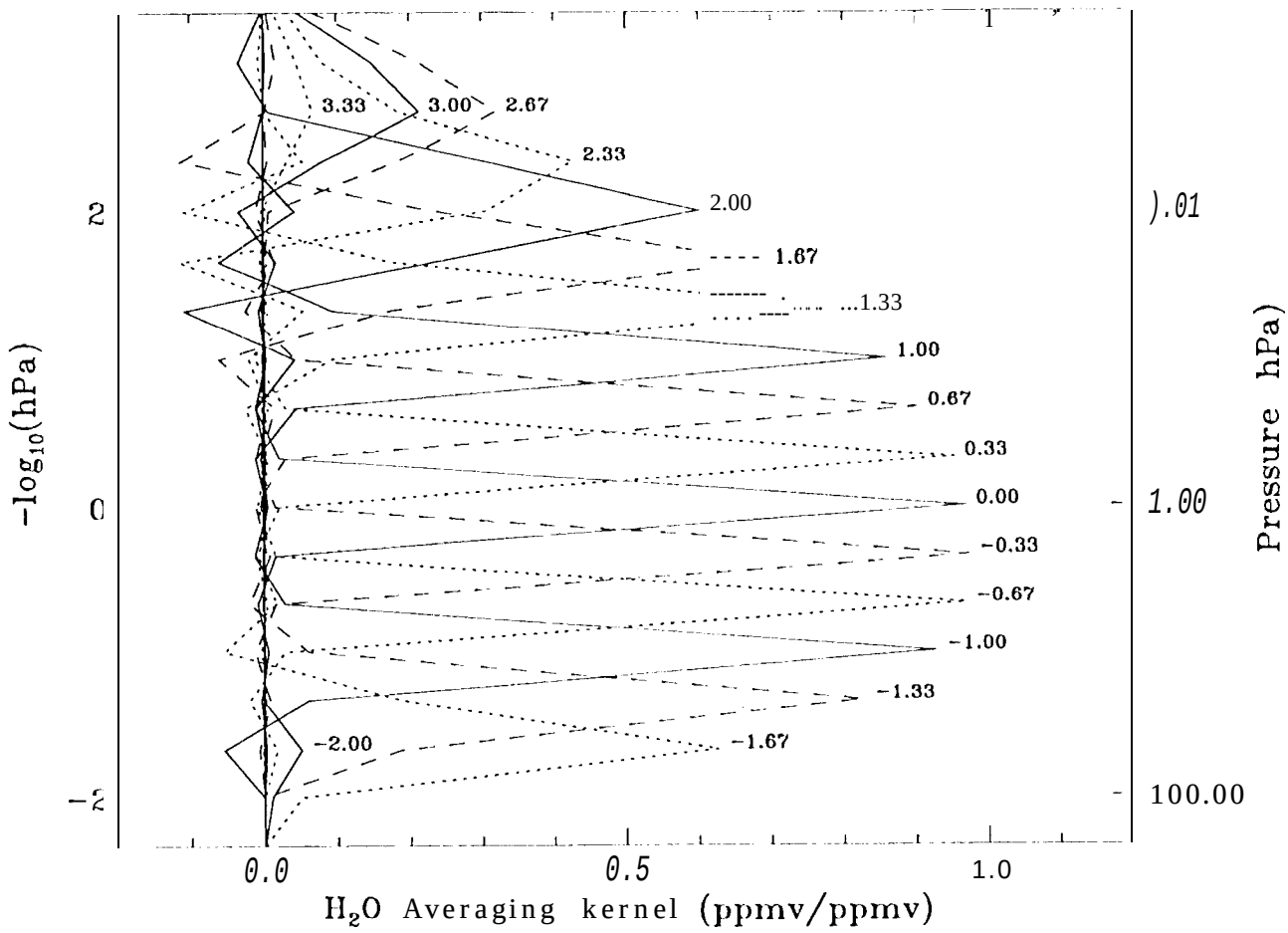
3.33
3.00
2.67
2.33
2.00
1.67
...1.33
1.00
0.67
0.33
0.00
-0.33
-0.67
-1.00
-1.33
-1.67
-2.00
2
0
-2
$-\log_{10}$(hPa)
).01
1.00
100.00
Pressure hPa)
0.0
0.5
1.0
H_2O Averaging kernel (ppmv/ppmv)

Fig 9

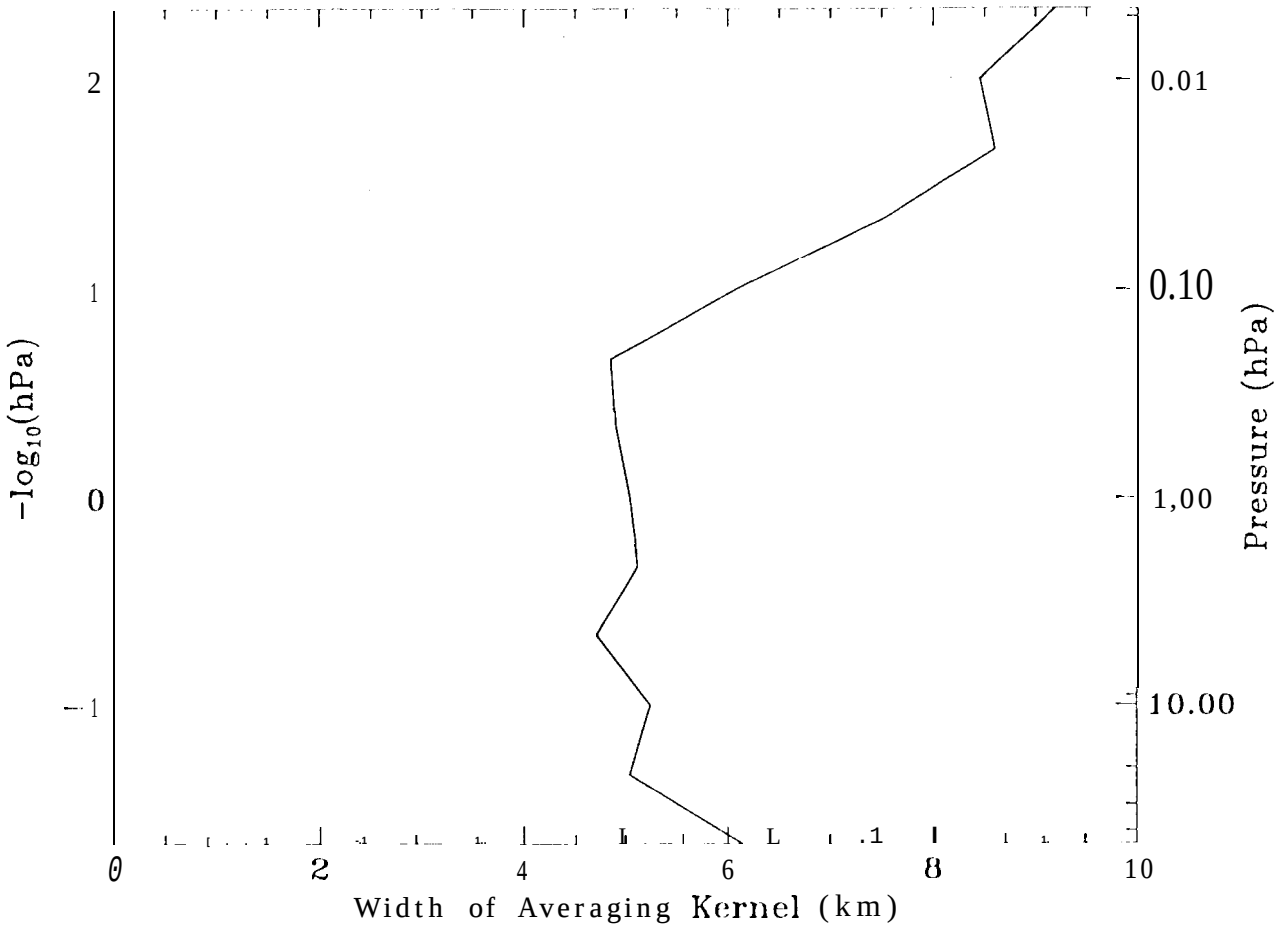
2
1
0
−1
$-\log_{10}$(hPa)
0.01
0.10
1.00
10.00
Pressure (hPa)
0
2
4
6
8
10
Width of Averaging Kernel (km)

Fig 10

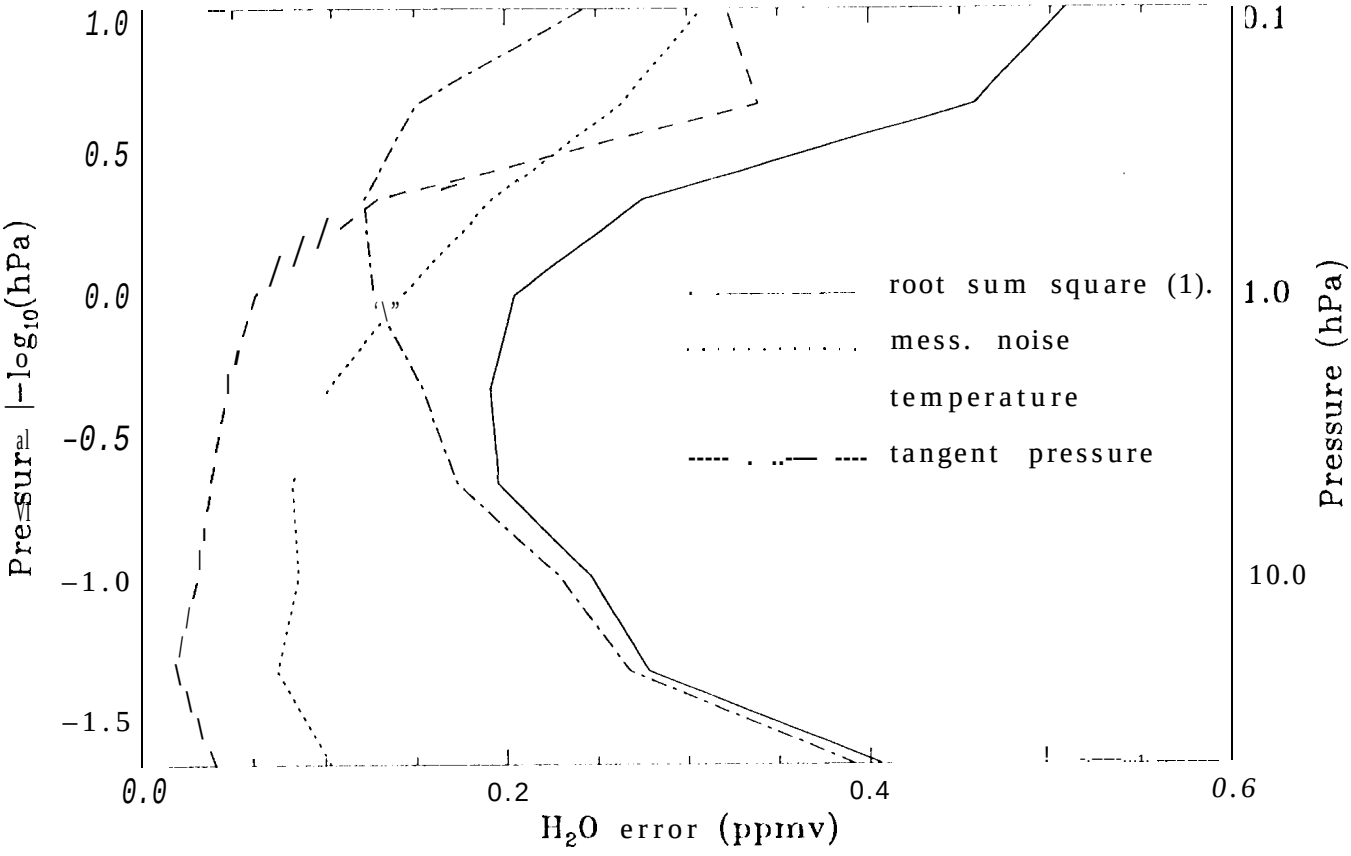
1.0
0.5
0.0
-0.5
-1.0
-1.5
Pressure $-\log_{10}$(hPa)
0.0
0.2
0.4
0.6
H_2O error (ppmv)
0.1
1.0
10.0
Pressure (hPa)
root sum square (1).
mess. noise
temperature
tangent pressure

Fig 11

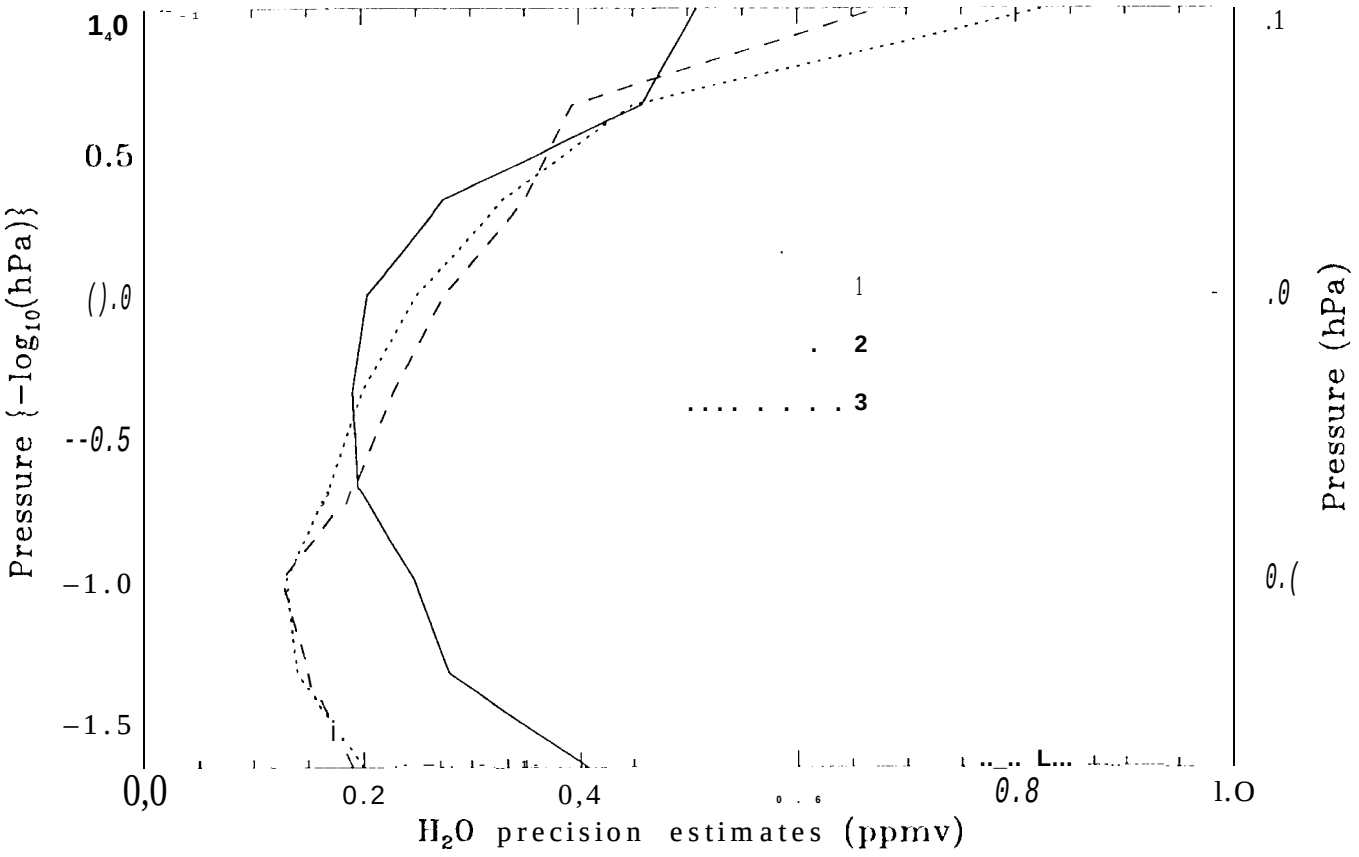
1,0
0.5
().0
--0.5
−1.0
−1.5
Pressure {−log10(hPa)}
.1
.0
0.(
Pressure (hPa)
1
2
3
0,0
0.2
0,4
0.8
1.O
H2O precision estimates (ppmv)

Fig 12

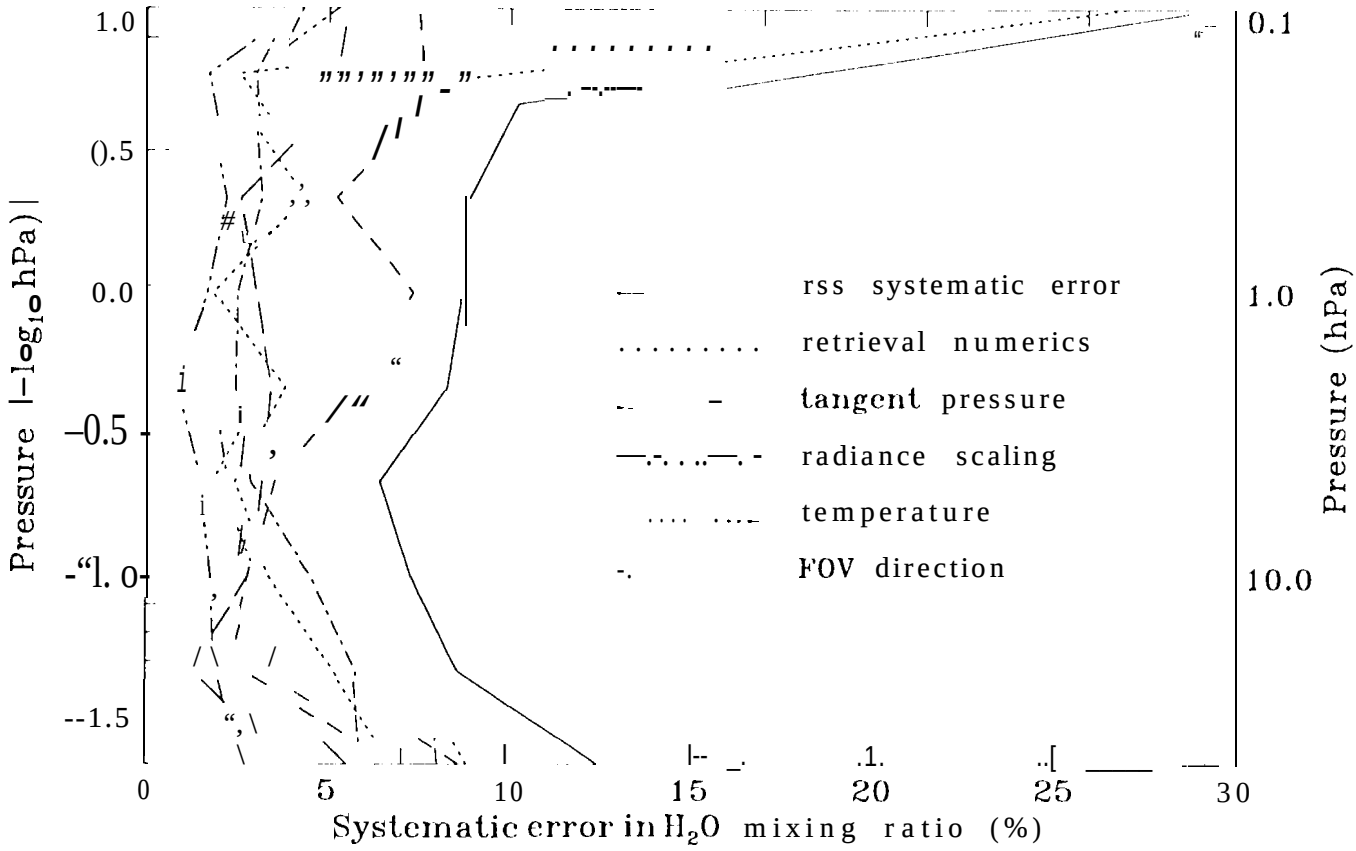
1.0
0.5
0.0
–0.5
-"l. 0
--1.5
Pressure |–log10 hPa)|
0.1
1.0
10.0
Pressure (hPa)
rss systematic error
retrieval numerics
tangent pressure
radiance scaling
temperature
FOV direction
0
5
10
15
20
25
30
Systematic error in H2O mixing ratio (%)

Fig 13

~~Fig 13~~

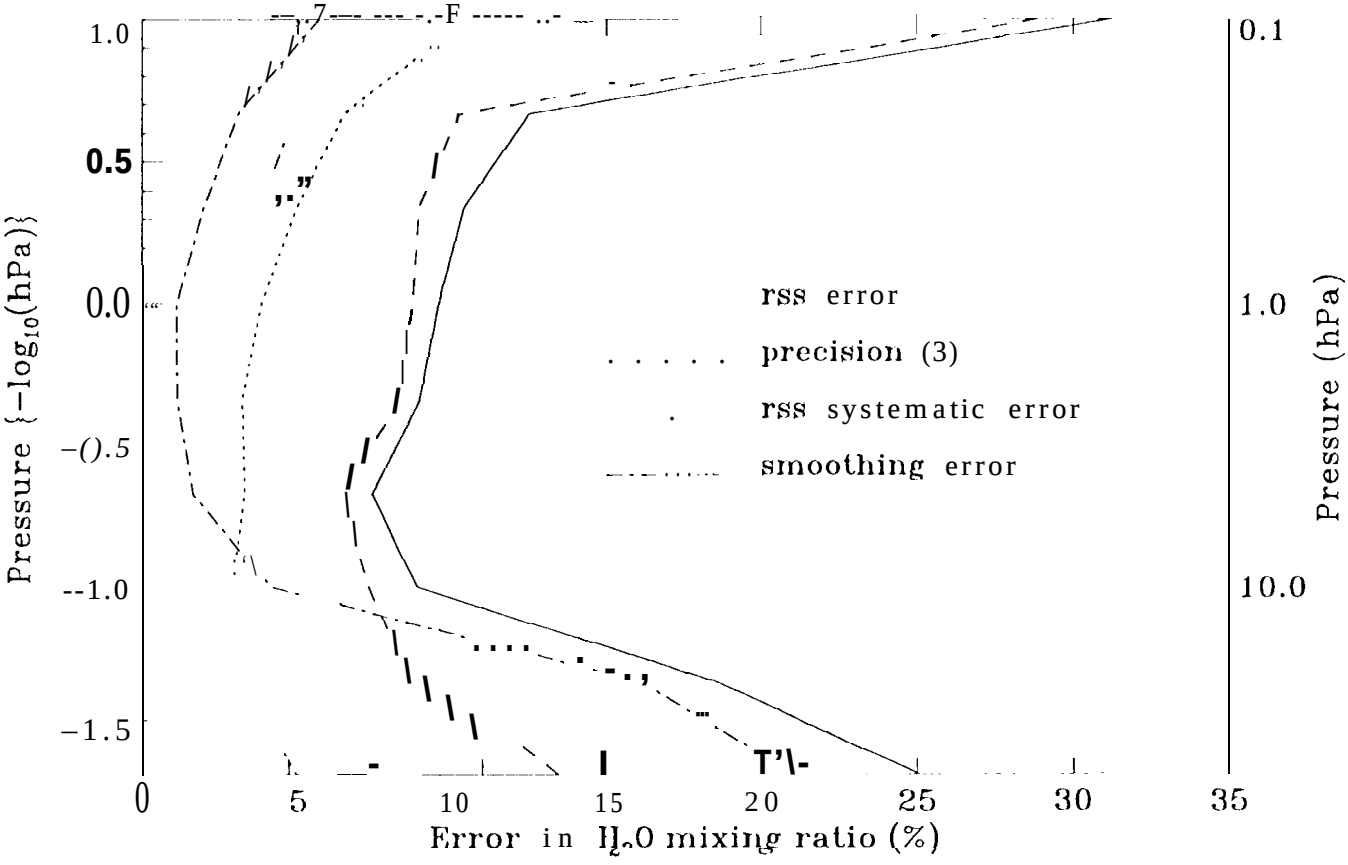
1.0
0.5
0.0
−0.5
−1.0
−1.5
Pressure {−log10(hPa)}
0.1
1.0
10.0
Pressure (hPa)
rss error
precision (3)
rss systematic error
smoothing error
0
5
10
15
20
25
30
35
Error in H2O mixing ratio (%)

log10(Pressure / hPa)
-2.0
-1.8
-1.6
-1.4
-1.2
-1.0
0
2
4
6
8
10
Water Vapour / ppmv
1000
10
Pressure / hPa

Fig 15

log10(Pressure / hPa)
[H2O] / ppmv
3
4
5
6
7
8
2
1
0
-1
1.000
0.100
0.010
0.001
Difference / ppmv
2
0
-2
Pressure / hPa

Fig 10

log10(Pressure / hPa)
-2.0
-1.5
-1.0
-0.5
0.0
2
4
6
8
Mixing Ratio [H2O] / ppmv
100
10
1
Pressure / hPa

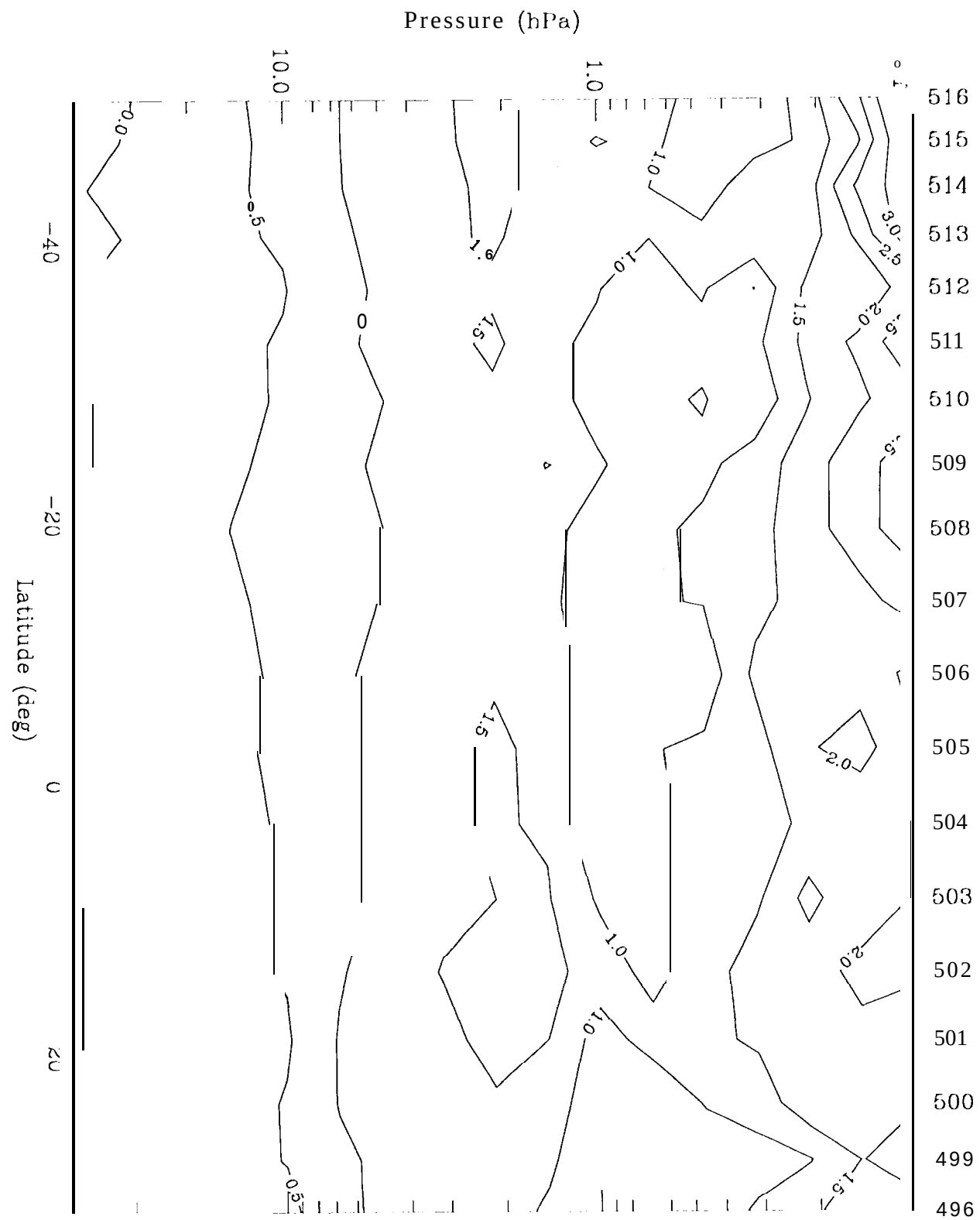
Pressure (hPa)
10.0
1.0
0.1
516
515
514
513
512
511
510
509
508
507
506
505
504
503
502
501
500
499
496
-40
-20
0
20
Latitude (deg)
0.0
0.5
0
1.6
1.5
1.0
1.5
1.0
1.0
1.5
2.0
2.5
3.0
2.0
1.5
1.5
2.0
1.0
1.0
2.0
0.5
1.5

Fig 18

UARS Standard Levels	Pressure (hPa)	Single Profile Precision (1) (ppmv)	(percent)	Accuracy (2) (ppmv)	(percent)
22	0.22	0.45	7	0.9	13
20	0.46	0.33	5	0.7	11
18	1	0.25	4	0.7	10
16	2.2	0.20	3	0.6	9
14	4.6	0.17	3	0.5	8
12	10	0.13	3	0.6	9
10	22	0.14	4	0.8	19
8	46	0.20	5	1.2	25

Table 1: MLS H_2O data summary. (1) The estimated precisions are based on the observed variability of retrievals in the tropics (see Method 3 of Estimated Precision in section § 4). (2) The estimated accuracies are based on the "1'01" analysis presented in s((-tie]] § 4.